Very large lepton collider in the Very Large Hadron Collider tunnel

Tanaji Sen
Fermi National Accelerator Laboratory, P.O. Box 500, Batavia, Illinois 60510

Jim Norem
HEP Division, Argonne National Laboratory, Argonne, Illinois 60439
(Received 11 May 2001; published 4 March 2002)

The Very Large Hadron Collider design is converging on a program where a 233 km circumference tunnel would first be occupied by a low field dipole system producing 40 TeV in the center of mass, followed by a higher field magnet system producing nearly 200 TeV in the center of mass. We consider the possibility of first using the tunnel for a large e^+e^- collider. We assume that the total radiated synchrotron power will be limited to 100 MW. We describe the design strategy, the luminosity and energy reach, the factors that limit the machine performance, the scaling laws that apply to its design, and the technology that would be required for its implementation.

DOI: 10.1103/PhysRevSTAB.5.031001 PACS numbers: 41.75.–i

I. INTRODUCTION

Plans for the future Very Large Hadron Collider (VLHC) now envisage a staging scenario [1] where a low field collider would be built first followed by a high field collider in the same tunnel several years later. There is also interest in an electron-positron collider in the same tunnel which could study physics that would complement the studies with the hadron collider. This machine could be used to (i) examine the W and Z^0 with high precision, to improve measurements of electroweak parameters by an order of magnitude, (ii) study continuum fermion pair production, (iii) produce clean Higgs mesons at an energy of perhaps 115 GeV, (iv) measure the W mass from W pair production thresholds, and (v) look at the $t\bar{t}$ thresholds with very good energy resolution [2]. The very large circumference of the tunnel makes it possible to think of an e^+-e^- ring which could reach an energy about twice that of the Large Electron Positron Collider (LEP) if we limit the synchrotron radiation power to 100 MW. Compared to the Next Linear Collider (NLC), the energy and possibly the luminosity reach of such a machine is lower. However, the energy resolution is better than that of the linear collider. The technology required is proven and available today. In this paper we outline the design of this Very Large Lepton Collider (VLLC) and consider some of the accelerator physics issues. We compare and contrast the parameters of this machine with LEP. Much of the material on LEP is obtained from a recent workshop on the subject of "e^+e^- in the VLHC" [3], and a recent paper by Brandt *et al.* [4]. Proceedings of the Chamonix workshops are also good sources of information on LEP. We attempt to identify the mechanisms that will limit the performance of the collider and look at scaling laws for the operation of such a machine at high energies. We also attempt to identify methods that could perhaps be used to both increase the performance of the machine and reduce the cost of the facility. Some aspects of this work were reported at the 2001 Particle Accelerator Conference [5] and the 2001 Snowmass Conference [6].

II. DESIGN STRATEGY

Our design philosophy of this electron-positron collider will be to make use of the maximum rf power available and operate at the beam-beam limit The synchrotron radiation power lost by *both beams*, each with beam current I, is

$$P_T = 2C_\gamma \frac{E^4 I}{e\rho}, \qquad C_\gamma = \frac{4\pi}{3}\frac{r_e}{(m_e c^2)^3} = 8.86 \times 10^{-5}\ [\mathrm{m/GeV^3}]. \tag{1}$$

Assuming that there are M_b bunches in each beam with bunch intensities N_b, the luminosity is

$$\mathcal{L} = \frac{f_{\mathrm{rev}}}{4\pi}\frac{M_b N_b^2}{\sigma_x^* \sigma_y^*}. \tag{2}$$

We will assume flat beams so that $\sigma_y^* \ll \sigma_x^*$. With this assumption, the vertical beam-beam tune shift is

$$\xi_y = \frac{r_e}{2\pi}\frac{N_b \beta_y^*}{\gamma \sigma_x^* \sigma_y^*}. \tag{3}$$

Eliminating one power of N_b from the expression for the luminosity, we can write

$$\mathcal{L} = \frac{1}{2er_e}\frac{\xi_y}{\beta_y^*}\gamma I, \tag{4}$$

where I is the beam current in a single beam. Our strategy, as stated earlier, is that as we change parameters, P_T and ξ_y will be held constant.

Using Eq. (4) to eliminate the current, we obtain the following equation for the luminosity and energy in terms of the fixed parameters and the bending radius ρ:

$$\mathcal{L}\gamma^3 = \frac{3}{16\pi r_e^2 (m_e c^2)}\frac{\xi_y P_T}{\beta_y^*}\rho. \tag{5}$$

This equation relates the parameters important to the physics program viz. the luminosity and energy to the machine size, optics, and beam parameters. For example, at constant luminosity this equation shows that the maximum allowable energy increases only with the cube root of the radius, the radiated power, or the beam-beam parameter. In the above equation β_y^* may be assumed constant at different energies only if the interaction region (IR) quadrupoles do not pose an aperture limitation in the vertical plane at any energy. We will assume that to be the case.

Similarly, Eq. (5) shows that the luminosity of the collider at a given energy and radiated power P_T can only be increased by increasing the beam-beam tune shift ξ_y and/or lowering β_y^*. Other limits can, however, prevent the machine from operating at the maximum theoretical luminosity, for example, limits on the maximum current in each bunch at injection.

A. Bunch intensity limitations

The dominant limitation on the bunch intensity at collision energy arises due to the beam-beam interactions. We have incorporated this constraint in our scaling of the luminosity with energy, Eq. (5). Another limitation that is more severe at injection energy is the transverse mode coupling instability (TMCI). As in the classical head-tail instability, synchrotron motion which exchanges particles in the head and tail of the bunch drives the instability, but this instability can arise even with zero chromaticity. In the presence of transverse impedances (typically wall resistivity), the wake forces excited by particles in the head can exert strong enough forces on the tail such that betatron modes $\omega_\beta + m\omega_s$ are modified. Typically, at the threshold intensity of the instability, the modes $m = 0$ and $m = -1$ become degenerate. TMCI is known to have limited the bunch current in LEP to below 1 mA [4]. A more extensive discussion of TMCI can be found in Ref. [7].

The threshold bunch current is given by

$$I_b^{\mathrm{TMCI}} \simeq \frac{8 f_{\mathrm{rev}} \nu_s E}{e \sum_i \beta_i k_{\perp i}(\sigma_s)}, \qquad (6)$$

where ν_s is the synchrotron frequency, the sum in the denominator is over transverse impedances, and $k_{\perp i}$ is a bunch length dependent transverse mode loss factor. Obviously higher synchrotron frequencies and longer bunches increase the threshold intensity. At LEP larger rf voltages were used to increase ν_s while emittance wigglers were used to increase the bunch length at the injection energy of 20 GeV. Compared to LEP, the Very Large Lepton Collider has a revolution frequency that is an order of magnitude smaller, while the synchrotron frequency, injection energy, and bunch length are comparable. If the impedances in LEP and this large ring are comparable, we may expect an order of magnitude reduction in the threshold current for this ring.

Keil [8] and Dugan [9] estimated the threshold current for this large collider following the model of LEP. The dominant sources of broadband impedance will be the rf cavities, bellows, and the resistive wall. LEP has bellows placed every 10 m around the ring. Assuming a similar placing and the same loss factors of the cavities and bellows as in LEP, the loss factor in the bellows would be an order of magnitude larger than that in the cavities. At a bunch length of 1 cm the threshold current would reduce to around 0.01 mA. The number of bellows therefore should be kept to a minimum. Improvements in the vacuum system design may in fact allow the complete elimination of these bellows or at least space them approximately every kilometer (see Sec. XI). In this case, the cavities and the resistive wall contribute about equally to the loss factor in this large ring. Dugan estimates that, at an injection energy of 46 GeV (this will be discussed in Sec. VIII) and in an elliptical chamber with aspect ratio of 2.5, the threshold current I_b^{TMCI} will be above 0.2 mA if the chamber half-height exceeds 4.8 cm. We will assume a design current of 0.1 mA to allow for a safety margin of 100%. It is worth noting that various schemes have been proposed to combat TMCI for the low-field hadron collider [10], e.g., starting with lower intensity bunches at injection energy and coalescing at higher energy, feedback systems, etc. If required, we may also use one of these compensation schemes to allow a bunch current of 0.1 mA.

B. Beam intensity limitations

The available rf power determines the beam current to zeroth order. This constraint will be used in the design strategy in this report. However, there are other sources of limitations which need to be considered as the design evolves. Perhaps the most important of these secondary limitations is the available cryogenic cooling power. We will assume that superconducting cavities will be used. The dynamic heat load on these cavities includes contributions from the rf dissipation and the beam induced heat load from both beams. These two sources lead to a power dissipation given by

$$P_{\mathrm{dynamic}} = N_{\mathrm{cav}} \frac{V_{\mathrm{rf}}^2}{(R/Q)Q} + 2R_m(\sigma_s) I_b I_e, \qquad (7)$$

where N_{cav} is the number of cavities, (R/Q) is the normalized shunt impedance per cavity, Q is the unloaded quality factor of the cavities which depends on the operating temperature and the field gradient, R_m is a bunch length dependent loss impedance of the cavities, I_b is the bunch current, and I_e is the single beam current. The available cryogenic power must be sufficient to cope with this load which has a contribution that increases with the beam current. The total higher order mode (HOM) power $P_{\mathrm{HOM}} \propto I_b I_e$ that could be absorbed by the superconducting cavities was another restriction on the total beam current at LEP. An upgrade of the couplers and rf cables was required to cope with

this limitation. Clearly, the design of the cavities for the future lepton collider should take advantage of the experience gained while operating LEP.

C. Synchrotron radiation power and beam-beam limited regime

Here we specify the design strategy keeping the beam-beam parameter and the synchrotron radiation power constant. The beam-beam parameter depends on the bunch intensity while the power depends on the beam intensity. Hence we will determine the bunch intensity N_b from ξ_y and the number of bunches M_b from P_T while ensuring that the maximum bunch intensity stays below the threshold required to avoid the transverse mode coupling instability.

Writing the emittances in the transverse planes as

$$\epsilon_y = \kappa \epsilon_x ,$$

where κ is the coupling ratio, the bunch intensity can be expressed as

$$N_b = \left(\frac{2\pi}{r_e} \sqrt{\frac{\kappa \beta_x^*}{\beta_y^*}}\, \xi_y \right) \gamma \epsilon_x , \tag{8}$$

where the factors within brackets are assumed to stay constant. One could imagine another scenario with optics changes where $\beta_x^*, \beta_y^*, \kappa$ are allowed to vary.

The equilibrium emittance ϵ_x is determined by the equilibrium between damping and quantum fluctuations and is given approximately by

$$\begin{aligned} \epsilon_x &= \frac{C_q}{J_x} \frac{R}{\rho} \frac{\gamma^2}{\nu_x^3} , \\ C_q &= \frac{55 \hbar c}{32\sqrt{3}\,(m_e c^2)} = 3.83 \times 10^{-13}\ \text{(m)} . \end{aligned} \tag{9}$$

Here R is the average radius of the arc assumed to be made of periodic structures such as FODO cells and ν_x is the arc tune. If L_c, μ_c are the length of each periodic cell and the phase advance over the cell, respectively, then

$$\nu_x = \frac{2\pi R}{L_c} \frac{\mu_c}{2\pi} = R \frac{\mu_c}{L_c} . \tag{10}$$

Hence,

$$\epsilon_x = \left(\frac{C_q}{J_x} \frac{R}{\rho} \left[\frac{L_c}{\mu_c} \right]^3 \right) \frac{\gamma^2}{R^3} . \tag{11}$$

The factor R/ρ—the ratio of the arc radius to the bend radius—can be treated as constant. Typically it has a value somewhere between 1.0 and 1.25. The arc radius is determined from the machine circumference C in terms of a filling factor f_1. Thus,

$$R = f_1 \frac{C}{2\pi} \quad \text{and} \quad \rho = f_2 R, \qquad f_1, f_2 < 1 , \tag{12}$$

where f_1, f_2 are held constant. Since we do not make optics changes at different stages, we will treat the factor in brackets in Eq. (11) as constant. The energy in this relation is of course determined from the energy luminosity relation Eq. (5). Once the emittance is known, the bunch intensity is calculated from Eq. (8).

The beam current I and the number of bunches are related as $I = e f_{\text{rev}} M_b N_b$, hence the maximum number of bunches is found from the total synchrotron radiation power as

$$M_b^{\max} = \left(\frac{P_T}{2 C_\gamma} \right) \frac{\rho}{f_{\text{rev}} N_b E^4} . \tag{13}$$

The factors in brackets are constant while the other factors change with the machine circumference.

D. rf parameters

There are two requirements on the rf voltage parameters. The first requirement on the voltage is that the energy gained due to the rf per turn must equal the energy lost per turn,

$$e V_{\text{rf}} \sin\phi_s = U = C_\gamma \frac{E^4}{\rho} , \tag{14}$$

where $C_\gamma = (4\pi/3) r_e/(m_e c^2)^3 = 8.86 \times 10^{-5}\ \text{m/GeV}^3$. The second requirement is that the rf acceptance ΔE_{rf} must be a certain number, say N_{QL}, times the rms energy spread σ_E for an acceptable quantum lifetime,

$$\Delta E_{\text{rf}} = N_{\text{QL}} \sigma_E , \tag{15}$$

or

$$\sqrt{\frac{1}{\pi h \eta_{\text{slip}}}\, e V_{\text{rf}} E G(\phi_s)} = N_{\text{QL}} \sqrt{\frac{C_q}{J_s \rho}}\, \frac{E^2}{m_e c^2} , \tag{16}$$

where

$$G(\phi_s) = 2\cos\phi_s - (\pi - 2\phi_s)\sin\phi_s . \tag{17}$$

J_s is the longitudinal damping partition number. Typically we require $N_{\text{QL}} \sim 10$. These two conditions can be solved to find the synchronous phase as the solution of the transcendental equation

$$\cot\phi_s + \phi_s - \frac{\pi}{2} - \frac{55\sqrt{3}}{256} \frac{h \eta_{\text{slip}}}{J_s \alpha_f} \frac{N_{\text{QL}}^2}{\gamma} = 0 , \tag{18}$$

where $\alpha_f = e^2/(4\pi\epsilon_0 \hbar c) = 1/137.04$ is the fine structure constant. This equation can be solved numerically. Once the synchronous phase is known, the rf voltage can be found from Eq. (14).

The rf frequency or the harmonic number is related to the desired bunch spacing. In order to accommodate both beams symmetrically around the ring, it is required that the bunch spacing be an even multiple of the rf wavelength. This in turn requires that the harmonic number be an even multiple of the number of bunches. The choice of rf frequency influences the energy acceptance $(\Delta E/E)_{\text{accep}}$ because $(\Delta E/E)_{accep} \propto 1/\sqrt{h}$ so lower rf frequencies increase the acceptance. However, two economical factors

argue for higher frequencies: (i) smaller frequencies increase the size and hence the cost of the cavity and (ii) high power klystrons are more cost effective above frequencies of 300 MHz. In superconducting cavities the frequency is limited from above by several factors: (i) cavity losses increase with frequency, (ii) longitudinal and transverse shunt impedances scale as $\omega_{\rm rf}$ and $\omega_{\rm rf}^2$, respectively, and (iii) the ratio of the energy removed by a bunch from the cavity to the stored energy in the cavity also increases with frequency. In this paper we will consider rf frequencies in the neighborhood of 352 MHz.

E. Optics

1. Arc optics

The choice of phase advance per cell μ_c and the length of a cell L_c are crucial design parameters. The equilibrium emittance decreases as the phase advance increases, reaches a minimum at 135°, and then increases again at larger values of μ_c. The horizontal dispersion also decreases with increasing phase advance and shorter cell lengths. Conversely, stronger focusing also increases the chromaticity and hence the strength of the sextupoles required to correct the chromaticity. Strong sextupoles can limit the available dynamic aperture. For these reasons, the choice of phase advance per cell in electron machines is usually limited in the range of $60° \le \mu_c < 120°$. For example, LEP started operation with $(60°, 60°)$ phase advances in the (x, y) planes at 46 GeV, and since then has used $(90°, 60°)$, $(90°, 90°)$, and $(102°, 90°)$ phase advances at higher energies.

Another parameter affected by the choice of optics is the threshold current for TMCI. From Eq. (6) we observe that $I_{\rm thresh}^{\rm TMCI} \propto \nu_s/(\sum_i \beta_i k_{\perp i})$. To estimate the dependence on μ_c, L_c we replace β_i by the average value in a FODO cell $\langle\beta\rangle = L_c/\sin\mu_c$. The synchrotron tune $\nu_s \propto \sqrt{\alpha_C}$, where α_C is the momentum compaction. Since $\alpha_C \propto 1/\sin^2(\mu_c/2)$, we find

$$I_{\rm thresh}^{\rm TMCI} \propto \frac{\nu_s}{\langle\beta\rangle} \propto \frac{1}{L_c}\cos\left(\frac{\mu_c}{2}\right). \tag{19}$$

Hence the TMCI threshold is raised with shorter cell lengths and smaller phase advance per cell.

In this paper we will choose the phase advance per cell $\mu_c = 90°$ and then choose a cell length L_c so that the bunch intensity does not exceed a certain threshold set by the TMCI. We will develop parameter sets (luminosity, energy, rf voltages, etc.) for different machine circumferences in this paper. As we increase the ring circumference, μ_c, L_c will be assumed constant while the revolution frequency decreases, and the bunch intensity always stays below the TMCI threshold.

The phase advance per cell is one way of controlling the equilibrium emittance. Another way is to redistribute the equilibrium emittance between the horizontal and longitudinal planes by changing the rf frequency. In a lattice constructed entirely of FODO cells, the change of partition number with momentum deviation is given by

$$\frac{dJ_x}{d\delta} = -\frac{dJ_s}{d\delta} = -4\,\frac{L_D}{L_Q}\left[\frac{2 + \frac{1}{2}\sin^2\mu_C/2}{\sin^2\mu_C/2}\right], \tag{20}$$

where L_D, L_Q are the length of dipoles in a half-cell and length of a quadrupole, respectively. Writing $J_x(\delta) = J_x(0) + (dJ_x/d\delta)\delta + \ldots$, we observe that reducing the emittance ϵ_x by half requires increasing the damping partition number to $J_x(\delta) = 2J_x(0)$ or a momentum shift of $\delta_{\Delta J_x=1} = 1/(dJ_x/d\delta)$ if initially $J_x(0) = 1$. The required rf frequency shift is related to the momentum deviation δ by

$$\frac{\Delta f_{\rm rf}}{f_{\rm rf}} = -\frac{\Delta R}{R} = -\alpha_C\delta\,. \tag{21}$$

While the horizontal emittance can be changed by an appropriate shift in rf frequency, there is also a change in the radial excursion ΔR of the beam. It is important to keep this as small as possible both to minimize a loss in physical aperture and to avoid a significant reduction in the transverse quantum lifetime. A lower phase advance per cell and a shorter quadrupole length relative to the dipole length, i.e., weaker focusing, help to keep the relative change in rf frequency and radial excursion small. As an example, we consider the 233 km ring whose parameters will be given in Sect. VI. With $L_D = 94.70$ m, $L_Q = 0.49$ m, $\mu_C = 90°$, and $\alpha_C = 0.23 \times 10^{-4}$, we find the damping aperture to be $\delta_{\Delta J_x=1} = 2.9 \times 10^{-4}$. The corresponding radial excursion is about $\Delta R = 0.20$ mm. Since this changes the damping partition number by one, we can write this as the change in damping partition per unit of radial excursion,

$$\frac{\Delta J_x}{\Delta R} = 5.0/\text{mm}\,.$$

Thus, radial excursions of the closed orbit by only fractions of a millimeter are sufficient to change the damping partition number by a unit or more.

An alternative method of reducing the transverse emittances is to place a damping wiggler in a region where the dispersion vanishes. Conversely, the emittance could be increased if required, e.g., to reduce the beam-beam tune shift, by placing the wiggler where the dispersion is nonzero.

If the horizontal emittance is reduced by any method, the energy spread increases, which decreases the energy resolution of the experiments, and the longitudinal quantum lifetime if the rf voltage is kept constant. This places constraints on the allowed emittance manipulations.

Synchrotron radiation in quadrupoles may be an issue. If the gradient is sufficiently large, particles with large betatron amplitudes may radiate enough energy that they are lost from the rf bucket. This was termed the radiative beta-synchrotron coupling (RBSC) [11]. A rough measure

of this effect [12] is the ratio of the field in a quadrupole at an amplitude equal to the rms beam size to the dipole bend field. To ensure that this effect is within bounds, the quadrupole gradient will be limited from above by requiring that this ratio not exceed unity.

2. Interaction region

A detailed design of the IR must include the focusing scheme to obtain the desired spot sizes, a beam separation scheme, the collimation and masking scheme to protect components from synchrotron radiation, local chromaticity correction if required, the interface with the detectors, etc. Here we will consider only the basic optics parameters. The lower limit on β^* is usually determined by the maximum tolerable beam size in the IR quadrupoles and the chromaticity generated by these quadrupoles. Furthermore, to prevent the loss of luminosity due to the hourglass effect, β^* should be significantly greater than the bunch length. A preliminary IR design [13] shows that it is possible to achieve $\beta_y^* = 1$ cm with sufficient momentum aperture. This was done with an IR design where the dispersion at the IP was made to vanish but the slope of the dispersion at the IP was allowed to be nonzero. Sextupoles placed next to the IR doublet quadrupoles start the chromaticity correction within the IR itself. A more precise estimate of the tolerable minimum β_y^* requires tracking to determine the dynamic aperture of the machine with realistic arc and IR magnets.

Here we will assume that $\beta_y^* \ll \beta_x^*$ as is true at most e^+-e^- rings. Consequently, aperture and chromaticity limitations will first arise in the vertical plane. As stated earlier in this section, we will consider fixed values of β_x^*, β_y^* at all circumferences and energies and assume that these do not pose aperture restrictions at any energy. These values will need to be reconsidered during the design of the final focusing system.

The choice of β_y^*/β_x^* needs to be closely related to the emittance coupling ratio $\kappa = \epsilon_y/\epsilon_x$. The horizontal beam-beam parameter is related to the vertical parameter as

$$\xi_x = \left[\sqrt{\frac{\kappa}{\beta_y^*/\beta_x^*}}\right]\xi_y\,. \tag{22}$$

If $\kappa > \beta_y^*/\beta_x^*$, $\xi_x > \xi_y$. In this case the beam-beam limit is reached first in the horizontal plane. Beyond this limiting current, the emittance grows linearly with current and the beam-beam parameters stay constant. In particular, the vertical beam-beam parameter ξ_y never reaches its maximum value and, since the luminosity is proportional to ξ_y, the maximum luminosity is not obtained. It is therefore desirable to have $\kappa \leq \beta_y^*/\beta_x^*$. In this paper we will consider the so-called *optimal coupling* scenario where $\kappa = \beta_y^*/\beta_x^*$ and the beam-beam limits are attained simultaneously in both planes, $\xi_x = \xi_y$.

F. Summary of design strategy

The design of the ring optics depends on a number of parameters, among these are the maximum synchrotron radiation power allowed by the facility, the maximum beam-beam parameter which is assumed, the number of IPs required to satisfy the user community (and saturate the tolerable beam-beam tune shift), and the maximum bunch intensity limited by TMCI. The minimum beta functions β_x^*, β_y^* at the interaction point and the emittance coupling ratio $\kappa = \epsilon_y/\epsilon_x$ must be specified. The arc design is determined by the arc filling factor f_1 and ring filling factor f_2, the phase advance per cell μ_C, and the required rf voltage determined by $N_{\rm QL}$—the ratio of rf bucket height (energy acceptance) to rms energy spread.

The design values for a first iteration can be produced from these requirements. For a given machine circumference C, determine the bend radius ρ and arc radius R from Eq. (12) with assumed values of f_1, f_2. The maximum energy of the ring at this circumference can then be determined from Eq. (5). The equilibrium emittance at this energy and required maximum bunch intensity from Eq. (8) can be calculated and compared with the maximum bunch current allowed by $I_{\rm thresh}^{\rm TMCI}$. The cell length can be obtained from Eq. (11). The maximum number of bunches can be obtained from Eq. (13). The maximum quadrupole gradient tolerable $B'_{\rm max}$ is found from

$$\frac{B'_{\rm max}\sigma_x}{B_0} = 1\,,$$

where σ_x is the rms horizontal beam size in the arcs and B_0 is the bend field. The values obtained must then be checked for internal consistency and collider performance.

III. LIFETIME

The radiative Bhabha scattering process $e^+e^- \rightarrow e^+e^-\gamma$ is expected to dominate the beam lifetime at collision in this large lepton collider. The lifetime from this process with a scattering cross section $\sigma_{e^+e^-}$ is

$$\tau_L = \frac{1}{N_{\rm IP}}\frac{M_b N_b}{\mathcal{L}\,\sigma_{e^+e^-}}\,. \tag{23}$$

Substituting for the luminosity from Eq. (4) we can write this in terms of the beam-beam parameter ξ_y as

$$\tau_L = \left[\frac{2r_e}{N_{\rm IP}}\frac{\beta_y^*}{\xi_y}\frac{1}{\sigma_{e^+e^-}}\right]\frac{1}{\gamma f_{\rm rev}}\,. \tag{24}$$

The cross section $\sigma_{e^+e^-}$ has a weak logarithmic dependence on energy [see Eq. (A24) in Appendix A] which can be ignored to first order. Assuming that β_y^*, ξ_y are constant, the terms in square brackets above can be considered nearly constant. At a fixed circumference, the luminosity lifetime decreases with approximately the first power of the energy.

There are other contributions to the beam lifetime such as beam-gas scattering and Compton scattering off thermal photons, but those lifetimes are about an order of

magnitude larger than the luminosity lifetime considered above. For present purposes those effects can be ignored but need to be considered at a later stage.

IV. SCALING OF THE BEAM-BEAM PARAMETER

Although a value of the beam-beam tune shift of $\xi_x \sim \xi_y \sim 0.03$–$0.06$ has described the operation of almost all lepton colliders over the past 20 years, recent results at LEP have shown that large colliders at high energies behave somewhat differently. The LEP machine operated at tune shifts around $\xi_x \sim \xi_y \sim 0.08$, and, in fact, did not reach the beam-beam limit when operated at energies around 100 GeV [14]. Since the machine described here is even larger and higher in energy than LEP, we consider how the LEP tune shifts can be extrapolated for operation at the highest energies.

Our use of the term "beam-beam limit" will be the conventional one. At this limit, the luminosity increases only linearly with beam intensity rather than quadratically and the beam-beam parameter reaches a constant value. There are other beam-beam related phenomena which can prevent this limit from being reached. These may be due to small dynamic aperture, growth of non-Gaussian tails, and coherent effects [14]. At LEP these phenomena were important at energies around 46 GeV but less so at higher energies. We assume that such effects are either negligible or adequately compensated in the following discussion.

The limiting value of the beam-beam parameter depends in a fundamental way on the damping time. The damping time τ_s determines the time it takes for the beam to reach an equilibrium distribution in the absence of external nonlinear forces. As the damping increases and this time decreases, the beam becomes more immune to nonresonant perturbations that would change this equilibrium distribution. Indeed, observations at several e^+–e^- colliders have shown that the limiting value of the beam-beam parameter increases slowly with energy or more precisely with the damping decrement. The damping decrement for beam-beam collisions is defined as the inverse of the number of beam-beam collisions per damping period,

$$\lambda_d = \frac{1}{N_{\rm IP}\tilde{\tau}_s} = \frac{C_\gamma E^3}{N_{\rm IP}\rho}, \tag{25}$$

where $\tilde{\tau}_s$ is the damping time measured in turns. There exists no reliable theory as yet that predicts how the beam-beam limit depends on λ_d. Keil and Talman [15] and more recently Peggs [16] considered the scaling of the beam-beam parameter with λ_d applied to data from earlier machines such as SPEAR, PETRA, and CESR and found roughly the power law behavior: $\xi_{y,\infty} \sim \lambda_d^{0.3}$.

In Appendix B we discuss a simple model where we treat the beam-beam kicks in the limit of high damping as random kicks analogous to the kicks produced by photon emission. The betatron phase is assumed to follow a white noise process as a consequence. As expected, this assumption overestimates the equilibrium emittance. If we soften this and allow for phase correlation which multiplies the correction by an undetermined factor less than unity, the beam-beam parameter depends on the bunch intensity as

$$\xi_y = \frac{2\xi_{y,0}}{1 + \sqrt{1 + 8\Gamma(N_b r_e/\gamma\epsilon_0)^2/\lambda_d}}, \tag{26}$$

where Γ is the undetermined fit parameter and $\xi_{y,0} = r_e\beta_y^* N_b/2\pi\gamma\sigma_x^*\sigma_y^*$ is the conventionally defined parameter. In the limit of small bunch intensity, $\xi_y = \xi_{y,0}$, while at large intensities,

$$\xi_{y,\infty} = \lim_{N_b\to\infty}\xi_y = \frac{1+\kappa}{2\pi}\sqrt{\frac{\beta_y^*}{\kappa\beta_x^*}}\sqrt{\frac{\lambda_d}{2\Gamma}}. \tag{27}$$

This asymptotic value depends only on the obvious lattice parameters, the damping decrement λ_d, and the fit parameter Γ, but is independent of the intensity.

In Ref. [17], Assmann and Cornelis, without specifying the model, wrote down the following expression for the beam-beam parameter in terms of the bunch current:

$$\xi_y = \frac{I_b}{\sqrt{A + (BI_b)^2}}. \tag{28}$$

The constant A is related to the emittances at zero current while the fit parameter B determines the asymptotic beam-beam parameter, $\xi_{y,\infty} = 1/B$. This expression (28) is close to but not exactly the same as Eq. (26). Using Eq. (28), Assmann and Cornelis find a good fit to the LEP data on the achieved beam-beam parameter at high energies. From this fit, the asymptotic beam-beam limit is inferred to be $\xi_{y,\infty} = 0.11$ at energies in the range 98–101 GeV. From this value and the observed beam-beam limit $\xi_{y,\infty} = 0.045$ at 45.6 GeV, a power law dependence is found as

$$\xi_{y,\infty} \propto \lambda_d^{0.4}. \tag{29}$$

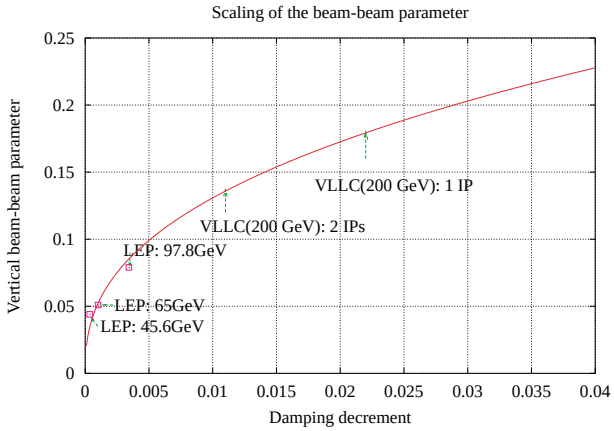

FIG. 1. (Color) Scaling of the asymptotic beam-beam parameter with the damping decrement when $\xi_{y,\infty} \propto \lambda_d^{0.4}$. The beam-beam parameters achieved at LEP are also shown. The beam-beam limit at LEP was reached only at the energy of 45.6 GeV. Assuming two IPs in the VLLC, $\lambda_d = 0.011$, $\xi_{y,\infty} = 0.137$ at 200 GeV, while if there is only one IP, then $\lambda_d = 0.022$, $\xi_{y,\infty} = 0.178$ also at 200 GeV.

We use this scaling law to determine the beam-beam limit at each energy of interest. Figure 1 shows this power law curve and also the expected beam-beam asymptotic limits for two cases in the VLLC at 200 GeV and a circumference of 233 km. The damping decrement assuming two IPs is 0.011, which implies $\xi_{y,\infty} = 0.137$, while with one IP $\lambda_d = 0.022$ and the expected $\xi_{y,\infty} = 0.178$. Note that LEP operated with 4 IPs, so the total beam-beam tune shift in LEP at the highest energies was around 0.3.

V. POLARIZATION

Electrons in a storage ring become vertically polarized via the emission of synchrotron radiation. In a perfect ring—planar and without errors—this polarization would build up to a maximum value of 92.4%. In a real ring—nonplanar, misalignments, and field errors—the maximum achievable polarization can be significantly less. The emission of photons with a very small probability of spin flip while leading to polarization also leads to depolarization in the presence of imperfections. The stochastic changes in electron energy after photon emission and coupling to the orbit motion lead to spin diffusion and loss of polarization. In the presence of depolarizing effects, the maximum value of the polarization along the equilibrium spin direction $\hat{n}$ is given by the expression due to Derbenev and Kondratenko [18]

$$P_\infty = -\frac{8}{5\sqrt{3}} \times \frac{\oint ds \langle \frac{1}{|\rho(s)|^3} \rangle \hat{y} \cdot (\hat{n} - \partial \hat{n}/\partial \delta) \rangle_s}{\oint ds \langle \frac{1}{|\rho(s)|^3} [1 - \frac{2}{9}(\hat{n} \cdot \hat{s})^2 + \frac{11}{18}(\partial \hat{n}/\partial \delta)^2] \rangle_s}, \tag{30}$$

where $\delta = \Delta p/p$ and $\langle \rangle_s$ denotes the average over phase space at a location s. We note that $\hat{n}$ is a vector field that changes with location in phase space. The polarization rate is approximately [19]

$$\frac{1}{\tau} = \frac{1}{\tau_{\rm ST}} + \frac{1}{\tau_{\rm dep}}, \tag{31}$$

$$\frac{1}{\tau_{\rm ST}} = \frac{8}{5\sqrt{3}} \frac{e^2 \gamma^5 \hbar}{m_e^2 c^2} \frac{1}{C} \times \oint ds \left\langle \frac{1}{|\rho(s)|^3} \left[1 - \frac{2}{9} (\hat{n}_0 \cdot \hat{s})^2 \right] \right\rangle_s, \tag{32}$$

$$\frac{1}{\tau_{\rm dep}} = \frac{8}{5\sqrt{3}} \frac{e^2 \gamma^5 \hbar}{m_e^2 c^2} \frac{1}{C} \oint ds \left\langle \frac{1}{|\rho(s)|^3} \frac{11}{18} (\partial \hat{n}/\partial \delta)^2 \right\rangle_s. \tag{33}$$

When $\hat{n}_0$ is nearly vertical, $\hat{n}_0 \cdot \hat{s}$ is small compared to unity and, assuming that the bend radius is everywhere the same, the Sokolov-Ternov polarization rate [20] reduces to the simplified expression

$$\frac{1}{\tau_{\rm ST}} \approx \frac{8}{5\sqrt{3}} \frac{e^2 \hbar}{m_e^2 c^2} \frac{\gamma^5}{\rho^3}. \tag{34}$$

The time to build up to the asymptotic polarization falls sharply with increasing energy but increases as the cube of the bend radius. The energy ratio between this collider and LEP is between 2–3, while the radius is nearly an order of magnitude larger than LEP. Consequently, the polarization build up time in this machine will be a few hours compared to approximately 6 min at 100 GeV in LEP. Polarization may still be a practical possibility, but that is primarily determined by the value of the achievable asymptotic polarization.

The key to calculating the asymptotic polarization P_∞ in a real machine lies in the calculation of the spin-orbit coupling vector $\partial \hat{n}/\partial \delta$. This depends on the detailed lattice configuration, and there are several sophisticated programs that do this [19,21].

Attaining the maximum polarization possible requires a combination of methods, as used, for example, in HERA [22] and LEP [23]. These include

(i) Tight alignment tolerances on all magnets, especially in the vertical plane.

(ii) Extremely good correction of the vertical closed orbit distortions and the vertical dispersion.

(iii) Careful selection of the tunes; e.g., the energy should be chosen so that the fractional part of the spin tune (approximately equal to $a\gamma$) is close to 0.5. At energies near 185 GeV, this would specify an energy of 184.84 GeV. The tunes in all planes should be chosen so that the resonance conditions

$$\nu_{\rm spin} = k + m_x \nu_x + m_y \nu_y + m_s \nu_s$$

are far from satisfied, especially for first order resonances $|m_x| + |m_y| + |m_s| = 1$, high order synchrotron sidebands to the integer resonances $m_x = m_y = 0$, and low order synchrotron sideband resonances of first order betatron resonances $|m_x| + |m_y| = 1$.

(iv) Harmonic spin matching and minimizing the spin orbit coupling will be essential. A sequence of vertical orbit correctors and dispersion correctors is used to generate harmonics that compensate the integer and linear spin resonances driven by the imperfection fields. These correction methods are more effective when each section of the ring is locally "spin transparent." This would place constraints on the phase advances and other Twiss functions in these sections.

Observations at several e^+-e^- rings have shown that the maximum polarization drops with energy. For electrons, integer resonances are spaced 0.44 GeV apart so the larger energy spread at higher energies leads to a larger portion of the resonance to be spanned by the beam distribution. However, prediction of the drop in polarization with energy is complicated and there does not exist a simple analytical way to extract the energy dependence of $\hat{n}$ in general. If, however, we assume that both orbital and spin

motion are approximately linear, examination of the spin-orbit coupling matrices (the **G** matrices in [19]) shows that $\partial\hat{n}/\partial\delta \propto \gamma^2$. Using Eq. (30) this implies [24,25] that the asymptotic polarization scales as

$$P_\infty = \frac{8}{5\sqrt{3}} \frac{1}{1 + \beta E^4}. \tag{35}$$

Here β is a parameter which does not depend on energy. Experience has shown that this relation is nearly true if the motion is linear and the closed orbit is well corrected. This scaling law will be violated if either the orbital motion or the spin motion is strongly nonlinear. Observations at LEP show a sharp falloff in polarization above 46 GeV and polarization at the level of a few percent at 60 GeV.

It is clear that, if polarization is desired, the lattice must be designed from the outset to achieve this. Further studies are required however to examine whether, even with the use of the methods outlined above, respectable levels of polarization will be achievable at the energies of interest. An initial study on expected polarization in this ring may be found in the paper by Assmann [26].

VI. DESIGN PARAMETERS AT HIGH ENERGY

The design strategy was outlined in Sec. II. We know, for example, that when the luminosity, synchrotron radiation power, and beam-beam parameters are fixed, the maximum energy of the beams scales with the cube root of the circumference. Here we apply this strategy to different machines with circumferences in the range from 200–300 km. This should span the range envisioned for different versions of the VLHC.

One feature of the design that needs some iteration is the initial choice of the beam-beam parameter. We saw in Sec. IV that the maximum beam-beam parameter scales with some power of the energy. Since the beam energy is an output parameter, we need to ensure that the choice of the beam-beam parameter is self-consistent with the design energy. In order to maximize the luminosity we will assume that there is a single IP in the ring.

Figure 2 shows the maximum energy as a function of the circumference for three different luminosities. For example, at a circumference of 233 km, the maximum single beam energies at luminosities of 10^{33}, 5×10^{33}, and 10^{34} cm^{-2} sec^{-1} are 602, 258, and 152 GeV, respectively. Thus a ring with circumference around 233 km should suffice to reach the top quark production threshold, estimated to be at 360 GeV, with a luminosity higher than 5×10^{33} cm^{-2} sec^{-1}. We observe that single beam energies from 570–650 GeV appear attainable at a luminosity of 10^{33} cm^{-2} sec^{-1}. However, the rf voltages required in

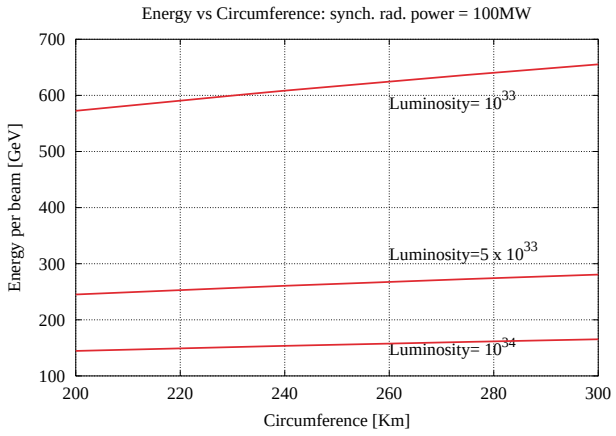

FIG. 2. (Color) The maximum energy attainable as a function of the machine circumference for three different luminosities. At the energies obtainable with luminosities of 10^{33} cm^{-2} sec^{-1} and lower, the maximum beam-beam parameter was set to 0.1. At the luminosity of 10^{34} cm^{-2} sec^{-1}, the beam-beam parameter was set to 0.05. The synchrotron radiation power of both beams was set to 100 MW in all cases.

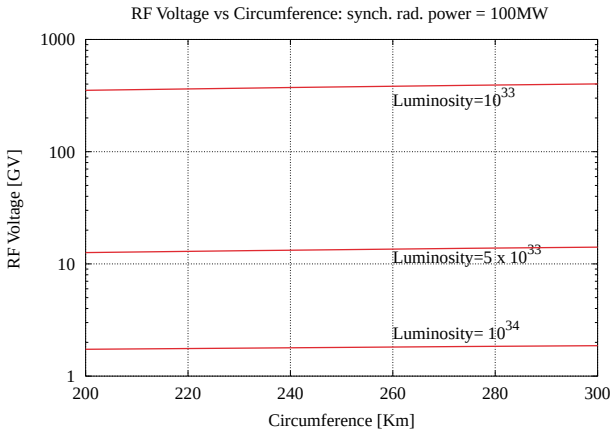

FIG. 3. rf voltage required *when operating at the maximum energy* as a function of the machine circumference for different luminosities with the synchrotron radiation power of both beams set to 100 MW in all cases.

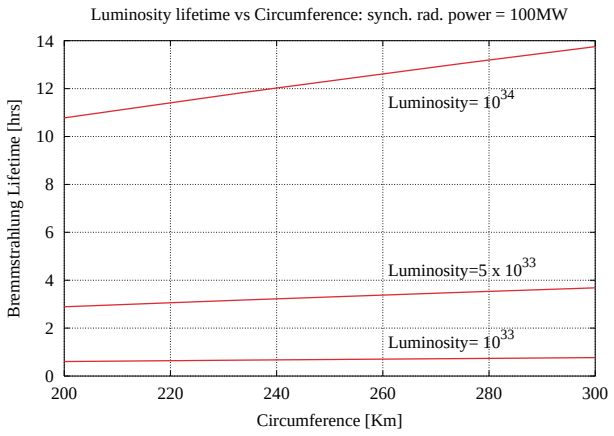

FIG. 4. Luminosity lifetime versus the circumference at three different luminosities. Here the lifetime *increases* with the required luminosity because the maximum energy decreases at higher luminosities and the lifetime $\sim 1/E$; cf. Eq. (24). See the text for other remarks.

this range of energies are in the hundreds of GV as seen in Fig. 3. In the range of 245–280 GeV per beam and luminosity 5×10^{33} cm^{-2} sec^{-1}, the rf voltages are a few GV, comparable to LEP.

Figure 4 shows the e^--e^+ bremsstrahlung lifetime as a function of circumference at three luminosities. The lifetime was calculated using the expression (A24) in Appendix A for the bremsstrahlung cross section. This expression does not have corrections from a cutoff parameter that correspond to the characteristic distance between particles in the bunches. With this cutoff, the cross sections are typically 30% lower. For example, analysis of the cross section at LEP energies [27] showed that the uncorrected cross section of 0.3 b was reduced to 0.2 b. This number was found to agree well with measurements. As a consequence of the smaller cross section, luminosity lifetimes may be about 30% higher than shown in Fig. 4. We observe that without this correction this lifetime is between 3–5 h at a luminosity of 5×10^{33} cm^{-2} sec^{-1} and energies between 245–280 GeV. By comparison, the luminosity lifetime at LEP was about 5–6 h.

Table I shows the design parameters at 200 GeV in a 233 km ring obtained by following the design strategy outlined in Sec. II. We remark on some of the interesting features of this ring compared to LEP.

(i) Increasing the circumference of LEP (by a factor of 8.5) and the total synchrotron radiation power (by about 7) while lowering the β_y^* (by a factor of 5) allows an increase in luminosity by almost 2 orders of magnitude at almost double the energy.

TABLE I. e^+-e^- collider parameters.

Parameter	LEP (1999)	VLLC
Circumference (m)	26 658.9	23 300.0
β_x^*, β_y^* (cm)	150, 5	100, 1
$\kappa/(\beta_y^*/\beta_x^*)$	0.31	1.0
Luminosity (cm^{-2} sec^{-1})	9.73×10^{31}	8.8×10^{33}
Energy (GeV)	97.8	200.0
Emittances ϵ_x, ϵ_y (nm)	21.1, 0.220	3.09, 0.031
rms beam size at IP σ_x^*, σ_y^* (μm)	178.0, 3.30	55.63, 0.56
Bunch intensity/current (/mA)	$4.01 \times 10^{11}/0.720$	$4.85 \times 10^{11}/0.10$
Number of bunches per beam	4	114
Bunch spacing (km)	6.66	2.04
Total beam current (both beams) (mA)	5.76	22.8
Beam-beam tune shift ξ_x, ξ_y	0.043, 0.079	0.18, 0.18
Number of IPs	4	1
e^+e^- bremsstrahlung lifetime (h)	6.0	4.8
Dipole field (T)	0.110	0.0208
Bend radius (m)	3026.42	32 073.17
Phase advance per cell μ_x, μ_y (deg)	102, 90	90.0
Cell length (m)	79.110	198.35
Total length of dipoles in a cell (m)	69	184.46
Quadrupole gradient (T/m)	9.50	20.0
Length of a quadrupole (m)	1.60	0.476
Arc $\sigma_x^{\max}, \sigma_x^{\min}$ (mm)	1.70, 0.60	1.02, 0.42
Arc dispersion $D^{\max}, D^{\min}$ (m)	1.03, 0.450	0.77, 0.37
Bend radius to machine radius $2\pi\rho/C$	0.710	0.86
Momentum compaction	1.60×10^{-4}	1.54×10^{-5}
Polarization time (h)	0.1	2.83
Energy loss per particle per turn (GeV)	2.67	4.42
Critical energy (keV)	686.0	514.6
Longitudinal damping time (turns)	73.0	45
rms relative energy spread	1.52×10^{-3}	9.57×10^{-4}
Bunch length (mm)	11.0	6.67
Synchrotron tune	0.116	0.082
rf voltage (MV)	3050.00	4852
rf frequency (MHz)	352.209	352
Revolution frequency (kHz)	11.245	1.287
Synchrotron radiation power (both beams) (MW)	14.5	100.7
Available rf power (MW)	34.1	
Power load from both beams (kW/m)	0.820	0.46
Photon flux/length from both beams (/m/sec)	2.40×10^{16}	0.91×10^{16}

(ii) The bunch current in VLLC is roughly 7 times lower in keeping with the expected lower threshold for TMCI.

(iii) The e^+-e^- bremsstrahlung lifetime in VLLC is slightly lower at 5 h. The ring will need to be refilled approximately every couple of hours in order to maximize the integrated luminosity.

(iv) The vertical beam sizes in the two machines are comparable. The horizontal beam sizes in the arcs of the two machines are also close. Hence vacuum chamber dimensions in the VLLC can be similar to those in LEP.

(v) The main dipole field is about 5 times weaker than that of LEP. Iron magnets operated at room temperature will suffice. Conversely, good shielding from stray magnetic fields, e.g., the earth's field, the fields of the low field hadron collider, will be critical.

(vi) The critical energy is smaller in VLLC so shielding against synchrotron radiation as in LEP should be adequate for VLLC. The photon flux per unit length is almost the same in the two machines.

(vii) The rf voltage required for VLLC is higher at 4.85 GV compared to 3.1 GV for LEP. We chose an energy acceptance that is 10 times the equilibrium energy spread of the beam to ensure sufficient quantum lifetime. At LEP, with the parameters given in Table I, this ratio is only about 6.6. If we assume this value for the 233 km ring, the rf voltage is lowered from 4.85 to 4.66 GV. The energy loss per turn requires that the rf voltage be greater than 4.4 GV.

(viii) We chose optimum coupling, i.e., $\epsilon_y/\epsilon_x = \beta_y^*/\beta_x^* = 0.01$ which implies that $\xi_x = \xi_y$. Operating at the beam-beam limit in both planes might well be challenging. If we reduce the emittance coupling to half this value, $\epsilon_y/\epsilon_x = 0.005$, then $\xi_x = 0.127$ while staying at the beam-beam limit in the vertical plane $\xi_y = 0.18$. With this choice, optics and beam size parameters change, e.g., $\epsilon_x = 4.4$ nm, cell length $= 222.6$ m, $\sigma_x^{\max} = 1.29$ mm, $D_x^{\max} = 0.97$ m, $\nu_s = 0.096$, and $\sigma_s = 7.2$ mm. The rf voltage increases to 4.92 GV while most other parameters are relatively unaffected.

VII. INSTABILITIES

Radio frequency cavities, the vacuum chamber, and bellows are likely to be the major sources of impedance in this ring. Beam position monitors, collimators, kickers, separators, synchrotron radiation masks, vacuum ports, etc. will be other sundry sources of impedance. A detailed impedance budget will be required as the design of these elements proceeds. Here we will consider only the major sources of impedance and the thresholds of likely instabilities. The instability growth rates will be evaluated at the injection energy of 46 GeV where they are the largest.

A. Transverse mode coupling instability

This instability determined by the transverse broadband impedance in the ring is the most important one and sets the upper limit on the single bunch current. Dugan's analysis [9] showed that a vacuum chamber half-height of 4.8 cm was required to obtain a threshold current of 0.2 mA at an injection energy of 46 GeV. The major assumption was that the bellows were placed no closer than 955 m so the loss factors from the bellows was limited to 100 $\mathrm{V\,pC^{-1}\,m^{-1}}$. The parameters of the ring have changed somewhat since that analysis so we will reconsider the limits on the vacuum chamber and the bellows.

The effective transverse impedance of the elliptical beam pipe is obtained by integrating the impedance $Z_\perp(\omega)$ over the bunch spectrum,

$$\mathrm{Im}[Z_\perp]_{\mathrm{eff}} = \frac{\int_{-\infty}^{\infty} \mathrm{Im}(Z_\perp) h_m(\omega)\, d\omega}{\int_{-\infty}^{\infty} h_m(\omega)}, \qquad (36)$$

where h_m is the bunch power spectrum of mode m. Since the modes coalesce at $m = 0$, we use $h_0 = \exp[-(\omega\sigma_t)^2]/(2\pi)$. After the integrations using an approximate expression for $Z_\perp$ for an elliptical beam pipe, the effective impedance is [9]

$$\mathrm{Im}[Z_\perp]_{\mathrm{eff}} \simeq -\frac{\Gamma(1/4)}{2\sqrt{2\pi^3}}\left(\frac{1}{b^3} + \frac{1}{a^3}\right) C\sqrt{c\mu_0\sigma_s\rho}\,, \quad (37)$$

where a, b are the half-height and half-width, respectively, of the vacuum chamber, C is the circumference, μ_0 is the permeability of vacuum, and ρ is the resistivity of the beam pipe material. The threshold current for the onset of TMCI due to the resistive wall impedance is

$$I_{\mathrm{thresh}}^{\mathrm{RW}} = \frac{16\pi\nu_s(E/e)}{\beta\,\mathrm{Im}[Z_\perp]_{\mathrm{eff}}}\frac{\sigma_s}{C} \simeq \frac{64\sqrt{2\pi^7}}{\Gamma(1/4)}\sqrt{\frac{\sigma_s}{c\mu_0\rho}}\frac{\nu_\beta\nu_s(E/e)}{C^3}\frac{1}{(1/b^3)+(1/a^3)}. \qquad (38)$$

The threshold currents due to the rf cavities and bellows are determined by using the loss factors $k_\perp$ of these elements,

$$I_{\mathrm{thresh}} \simeq \frac{8\nu_s f_{\mathrm{rev}}(E/e)}{\langle\beta\rangle\sum k_{\perp,i}(\sigma_s)}. \qquad (39)$$

The loss factors as measured at LEP are about 2.3 $\mathrm{V\,pC^{-1}\,m^{-1}}$ at $\sigma_s = 1$ cm for a 10 MV superconducting cavity and about 0.41 $\mathrm{V\,pC^{-1}\,m^{-1}}$ at $\sigma_s = 1$ cm for a single bellows. The net threshold current from these three sources is

$$\frac{1}{I^{\mathrm{thresh}}} = \frac{1}{I_{\mathrm{thresh}}^{\mathrm{RW}}} + \frac{1}{I_{\mathrm{thresh}}^{\mathrm{rf}}} + \frac{1}{I_{\mathrm{thresh}}^{\mathrm{bellows}}}. \qquad (40)$$

We will consider two different materials for the beam pipe, aluminum and copper, and two values for the total loss factor of the bellows, 100 and 300 $\mathrm{V\,pC^{-1}\,m^{-1}}$. The larger value would correspond to bellows placed about every 318 m apart. Table II shows the relevant parameters for the calculation of the threshold current. The number of cavities is determined by the voltage of 4852 MV required for operation at 200 GeV. We assume that each cavity supplies 10 MV leading to a total of about 486 cavities. The

TABLE II. Parameters used in the calculation of the TMCI threshold current.

ρ_{Al} (Ωm)	2.65×10^{-8}
ρ_{Cu} (Ωm)	1.7×10^{-8}
a	$= 2.5b$
Number of rf cavities	486
$k_{\perp}^{\mathrm{rf}}$ (V pC^{-1} m^{-1})	1118
$k_{\perp}^{\mathrm{bellows}}$(V pC^{-1} m^{-1})	100/300
$\langle\beta\rangle$ (m)	133
E (GeV)	46.0
σ_s (cm)	1.22
ν_s	0.108

bunch parameters ν_s, σ_s are the values at injection energy 46 GeV.

Figure 5 shows the threshold current I_{thresh} as a function of the half-height b for the different cases. If a copper coating on the beam pipe is essential, for example to minimize parasitic heating and eddy current losses, then the threshold current of 0.2 mA is obtained at $b = 4.6$ cm when $k_{\perp}^{\mathrm{bellows}} = 100$ V pC^{-1} m^{-1} and at $b = 5.0$ cm when $k_{\perp}^{\mathrm{bellows}} = 300$ V pC^{-1} m^{-1}. With an aluminum beam pipe, the corresponding values are $b = 4.8$ cm when $k_{\perp}^{\mathrm{bellows}} = 100$ V pC^{-1} m^{-1} and $b = 5.4$ cm when $k_{\perp}^{\mathrm{bellows}} = 300$ V pC^{-1} m^{-1}. The resistive wall impedance, with either Al or Cu, is the dominant contribution to the transverse impedance when the chamber half-height is less than 3 cm. At larger chamber heights the choice of the material and the impedance of the bellows start to make a difference. There is therefore room to optimize on the cost and complexity of the vacuum chamber design. The demands on the vacuum chamber size would be reduced if bunches could be coalesced after reaching top energy. This needs to be studied further.

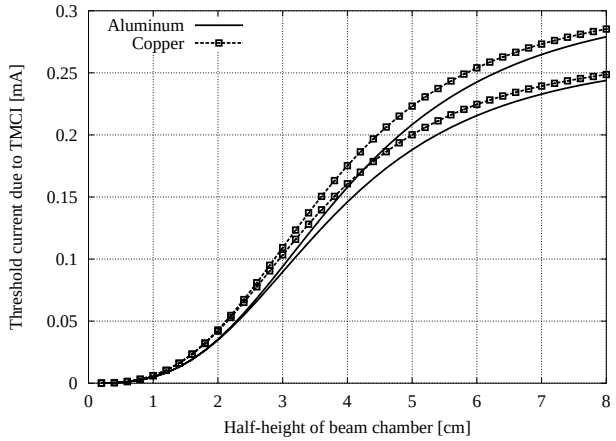

FIG. 5. Threshold current for the onset of TMCI as a function of the vacuum chamber half-height. We consider aluminum and copper as the material of the beam pipe. For each case, we consider two possible values of $k_{\perp}^{\mathrm{bellows}}$: the top curve for each material corresponds to $k_{\perp}^{\mathrm{bellows}} = 100$ V pC^{-1} m^{-1} and the bottom curve corresponds to $k_{\perp}^{\mathrm{bellows}} = 300$ V pC^{-1} m^{-1}.

B. Longitudinal mode coupling instability

This is also known as the longitudinal microwave instability [28]. It usually does not lead to beam loss but to growth in the bunch length and energy spread up to a point before leveling off. The onset of this instability occurs when the $m_s = 2$ sideband coalesces with the $m_s = 1$ sideband. The threshold for bunched beams is given by the Keil-Schnell-Boussard criterion [29],

$$\left[\frac{Z_{\|}}{n}\right]_{\mathrm{eff}} = \frac{2\pi|\eta|\,(E/e)\,(\sigma_p)^2}{\hat{I}}, \tag{41}$$

where η is the slip factor and $\hat{I} = \sqrt{2\pi}\, cI_{\mathrm{av}}/(\omega_{\mathrm{rev}}\sigma_s)$ is the peak bunch current. For short bunches $\sigma_s < b$ (as is the case for the VLLC), the effective impedance is reduced and can be modeled by the SPEAR scaling ansatz [30]

$$\left[\frac{Z_{\|}}{n}\right]_{\mathrm{eff}}^{\mathrm{short}} = \left[\frac{Z_{\|}}{n}\right]_{\mathrm{eff}}\left(\frac{\sigma_s}{b}\right)^{1.68}. \tag{42}$$

With this scaling taken into account, the threshold impedance for the onset of this instability is 3.39 mΩ.

We evaluate the effective longitudinal impedance of the ring due to the resistive wall. The effective impedance is

$$\left[\frac{Z_{\|}}{n}\right]_{\mathrm{eff}} = \frac{\int_{-\infty}^{\infty}(Z_{\|}/n)h_m(\omega)\,d\omega}{\int_{-\infty}^{\infty}h_m(\omega)}. \tag{43}$$

Since the instability develops near $m = 1$, the impedance should be evaluated at this frequency. Using $h_1 = (\omega\sigma_t)^2\exp[-(\omega\sigma_t)^2]/(4\pi)$ and doing the integrations, we find

$$\left[\frac{Z_{\|}}{n}\right]_{\mathrm{eff}} = \frac{\Gamma(1/4)}{2\sqrt{\pi}}\,\frac{R\rho(1/b + 1/a)}{2\delta_1}\sqrt{\frac{\omega_{\mathrm{rev}}}{\omega_{\mathrm{bunch}}}}, \tag{44}$$

where δ_1 is the skin depth at the revolution frequency and $\omega_{\mathrm{bunch}} = c/\sigma_s$. This expression amounts to a roughly

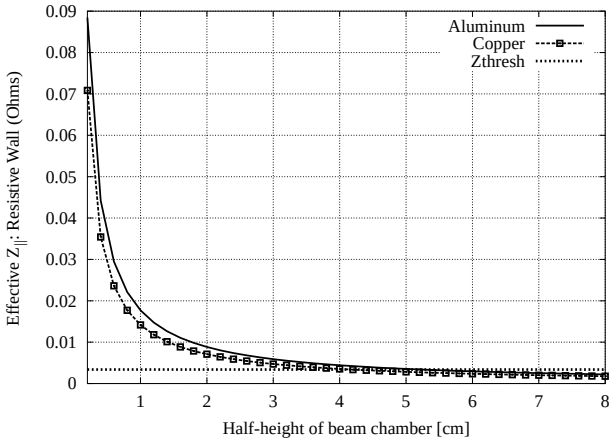

FIG. 6. The effective longitudinal impedance due to the resistive wall as a function of the vacuum chamber half-height for aluminum and copper. The line $Z_{\mathrm{thresh}} = 3.39$ mΩ corresponds to the threshold impedance for the onset of the microwave instability.

2% correction on simply evaluating the resistive wall impedance at the frequency ω_{bunch}.

Figure 6 shows the effective impedance as a function of the half-height. The wall impedance is lower than the threshold impedance only for half-heights greater than 5 cm for both aluminum and copper. When other sources of impedance are included, the ring impedance will exceed the threshold for the onset of the microwave instability. As mentioned earlier, this is not devastating. For example, with the rf voltage set to provide an rf acceptance of 10 times the equilibrium energy spread, the quantum lifetime should be sufficient even with the increased momentum spread.

C. Transverse coupled bunch instabilities

A transverse coupled bunch mode is described by two mode numbers (m, n). With M equally spaced bunches, there are M coupled bunch modes with mode numbers $m = 0, 1, \ldots, M - 1$. The index n describes the motion of individual bunches in synchrotron phase space, thus $n = 0$ describes rigid dipole motion of the bunch, in the $n = 1$ mode the head and tail are out of phase transversely, etc. At zero current, the frequency of mode (m, n) is $(\nu_\beta + n\nu_s)\omega_{\text{rev}}$.

The growth rate for the (m, n)th mode is [28]

$$\frac{1}{\tau_\perp^{(m,n)}} = -\frac{1}{1 + m}\,\frac{cMI_b}{4\pi\nu_\beta(E/e)} \times \sum_k \text{Re}Z_\perp[(kM + m + \nu_\beta + n\nu_s)] \times F'_m(\omega\tau_t - \chi), \quad (45)$$

where F'_m is a form factor depending on $\tau_t = 2\sqrt{6}\,\sigma_t$, the total length (in time) of a Gaussian bunch, and $\chi = \nu'_\beta\omega_{\text{rev}}\tau_t/\eta$. ν'_β is the chromaticity. The mode with the fastest growth rate is the $n = 0$ mode.

The resistive wall contributes to this instability. As $\omega \to 0$ the resistive impedance increases as $|\omega|^{-1/2}$ (as long as the wall thickness is greater than the skin depth). The mode with the largest growth is the one with the negative frequency closest to zero, $kM + m + \nu_\beta \approx 0$. With $M = 114$ and $\nu_\beta = 279.4$, this would correspond to the mode with $k = -3$ and $m = 62$. The form factor F'_0 is approximately unity for zero chromaticity, so we obtain the growth rate for the fastest mode,

$$\frac{1}{\tau_\perp^{(62,0)}} = \frac{cMI_b}{4\pi\nu_\beta(E/e)}\,\frac{cC}{2\pi}\left(\frac{1}{b^3} + \frac{1}{a^3}\right)\sqrt{\frac{\mu_0\rho}{4\pi\Delta\nu_\beta\omega_{\text{rev}}}}, \quad (46)$$

where $\Delta\nu_\beta$ is the betatron tune difference below the integer. Setting $\Delta\nu_\beta = 0.1$ to obtain the fastest rate, we obtain a growth time of 117 msec or 151 turns at 46 GeV.

TABLE III. HOMs in the 352 MHz LEP SC cavities [31].

Frequency (MHz)	R/Q (Ω)	Q
	Transverse	
461	18	16 000
476	15	14 000
506	20	16 500
639	56	11 500
688	25	6000
	Longitudinal	
513	13	44 000
1006	16	5500

TABLE IV. Fastest growth rates of transverse coupled bunch modes due to rf cavity HOMs.

Mode number n	Mode number m	Growth time (sec) ($E = 46$ GeV)
0	62	0.14
0	61	0.23
0	60	0.29
1	93	210.7
1	92	2110.5

The individual HOMs of the rf cavities will also contribute strongly to the wakefields coupling several bunches. As a worst case estimate we will assume that the HOMs of different cavities coincide exactly. Neglecting the spread in frequencies due to the fabrication process will lead to the fastest growth rates. We will use the HOM frequencies and corresponding R/Q and Q values for the superconducting LEP cavities which operate at 352.209 MHz. These cavities have dominant HOMs clustered around 480, 650, and 1100 MHz [31]. HOM couplers are designed to extract the energy at these modes from the cavity and reduce the impedance at these frequencies. Table III (taken from Ref. [31]) shows the dominant cavity modes and the impedances achieved with the use of these couplers.

We use the program ZAP [32] to estimate the growth rate for some of the fastest modes. Table IV shows that the shortest growth times due to the cavity HOMs are of the same order as that due to the resistive wall. Note that these growth times are smaller than the transverse radiation damping time of about 3700 turns or 5.7 secs at 46 GeV. If the betatron frequency spread is not enough to Landau damp these modes, a feedback system will be necessary to damp the transverse coupled bunch instability.

D. Longitudinal coupled bunch instabilities

As in the transverse coupled bunch case, two mode numbers (m, n) are required. Now $n = 1$ describes rigid dipole motion, $n = 2$ describes quadrupole motion of the bunch, etc. At zero current, the frequency of mode (m, n) is $n\nu_s\omega_{\text{rev}}$.

The growth rate is determined by the resistive part of the impedance [33],

$$\frac{1}{\tau_\parallel^{m,n}} = \frac{\eta h\omega_{\text{rev}}I_{\text{av}}}{4\pi\nu_s(E/e)}\,\frac{\sum_k h_m(\omega_k)\,\text{Re}(Z_\parallel[\omega_k])/\omega_k}{\sum_k h_m(\omega_k)}, \quad (47)$$

TABLE V. Fastest growth rates of longitudinal coupled bunch modes due to rf cavity HOMs.

Mode number n	Mode number m	Growth time (sec) ($E = 46$ GeV)
1	25	0.022
1	26	3.04
1	24	3.53
2	25	2.70
2	26	443.8

where $\omega_k = (kM + m + n\nu_s)\omega_{\rm rev}$. The reactive part of the impedance determines the coherent frequency shift. Unlike the transverse case, the resistive wall impedance at low frequency does not contribute to the longitudinal instability because even the lowest bunch spectrum function h_1 vanishes faster than the impedance increases as $\omega \to 0$. Table V shows the most unstable modes determined using ZAP with the rf HOMs shown in Table III. The growth time of the most unstable mode is only 0.02 sec, which is faster than the transverse multibunch instability growth rate. If the combination of Landau damping due to a synchrotron frequency spread and radiation damping is not enough, a longitudinal feedback system will be necessary.

VIII. A COLLIDER AT 46 GEV

There is considerable interest in precision measurements at the W and Z^0 mass range, $E_{\rm CM} \sim 90$ GeV. Here we consider the feasibility of using this large collider to attain high luminosities—in excess of 5×10^{33} cm^{-2} sec^{-1}. These are the so-called "gigaZ" measurements which required integrated luminosities around 500 inverse picobarns. Polarized beams at this energy will greatly add to the physics program allowing for example measurements of the left-right asymmetry or the Weinberg angle.

The design principles for obtaining high luminosity at low energies are different from those at high energy. At low energies, the synchrotron radiation power is low and does not impose any constraints. Only the beam-beam tune shift limit needs to be respected. This constrains the bunch intensity per unit transverse area or N_b/ϵ. Under these conditions, the luminosity is

$$\mathcal{L} = \frac{\pi}{r_e^2} M_B f_{\rm rev} \left[\frac{\sigma_x^* \sigma_y^*}{(\beta_y^*)^2} \right] \gamma^2 \xi_y^2 , \tag{48}$$

$$= \frac{\pi}{r_e^2} M_B f_{\rm rev} \left[\frac{\kappa \beta_x^*}{(\beta_y^*)^3} \right]^{1/2} \gamma^2 \xi_y^2 \epsilon_x . \tag{49}$$

In this regime the luminosity increases with the emittance $\mathcal{L} \propto \epsilon_x$, so this requires that the aperture be filled to maximize the luminosity. Leaving enough room for good quantum lifetime, the maximum permissible emittance could be determined by a condition such as

$$A_{\rm req} \equiv 10 * [\sigma_x^2 + (D_x \delta_p)^2]^{1/2} + \text{c.o.d.} \le r_{\rm pipe} , \tag{50}$$

where c.o.d. is the expected closed orbit distortion and $r_{\rm pipe}$ is the radius of the beam pipe. The emittance can be increased by lowering the phase advance per cell. The bunch intensity is found from the beam-beam tune shift

$$N_b = \left(\frac{2\pi}{r_e} \sqrt{\frac{\kappa}{\beta_y^*/\beta_x^*}} \right) \gamma \epsilon_x \xi_y . \tag{51}$$

If this intensity exceeds the TMCI threshold $N_b^{\rm TMCI}$, the emittance can be lowered by increasing the phase advance.

There is no significant constraint on the beam current from the synchrotron radiation power so this does not limit the number of bunches. Instead, the number of bunches is limited by the minimum bunch spacing allowed. This spacing $S_b^{\rm min}$ could be limited by multibunch instabilities. Assuming a uniform bunch distribution around the ring, the number of bunches is determined by

$$M_B f_{\rm rev} = \frac{c}{S_b^{\rm min}} . \tag{52}$$

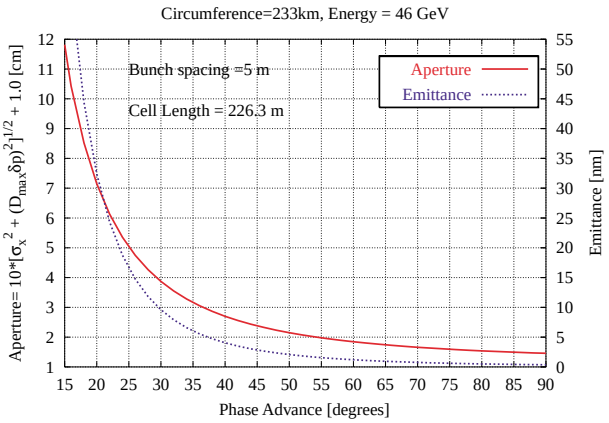

(a)

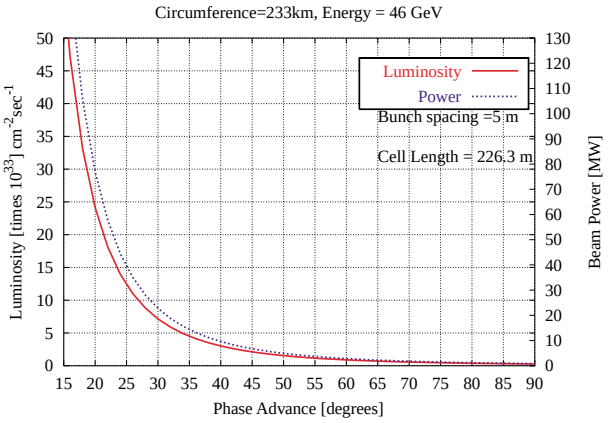

(b)

FIG. 7. (Color) (a) The emittance and $A_{\rm req}$ as a function of the phase advance per cell. Assuming the beam pipe radius is 5 cm, this determines the minimum phase advance to be 25°. (b) The luminosity and synchrotron radiation power as a function of the phase advance. The luminosity drops below 10^{34} cm^{-2} sec^{-1} at phase advances greater than 27°.

We will assume $S_b^{\min} = 5$ m, somewhat arbitrarily. It remains to be checked that such a short bunch spacing is feasible with a reasonable longitudinal feedback system.

For 46 GeV operation we will use the same magnet lengths as determined by high energy operation. The cell length is also fixed although it may be attractive to double the cell length by turning off one-half (or perhaps two-thirds) of the quadrupoles. This would allow a higher phase advance for the same emittance. We assume that the beam pipe radius is 5 cm. High energy operation fixes some of the ring parameters. These include the average arc and bend radius, length of the magnets, and FODO cells

The minimum phase advance per cell $\mu^{\min}$ is determined by the requirement $A_{\text{req}} \leq 5$ cm. We allow for a rms closed orbit distortion of 1 cm—a conservatively large value. Figure 7(a) shows the emittance and A_{req} as a function of the phase advance. From this figure we determine $\mu^{\min} = 25°$. Figure 7(b) shows that the luminosity drops below 10^{34} cm^{-2} sec^{-1} at phase advances greater than 27°. Hence we set the phase advance per cell to the minimum value $\mu_C = \mu^{\min}$. The values of other parameters follow and are shown in Table VI.

The luminosity is slightly above 10^{34} cm^{-2} sec^{-1}. The single bunch current is low at 0.03 mA or about one-third of that required at 200 GeV so the TMCI instability may not be an issue. However, with the large number of bunches, the beam current is high at 1.4 A. This makes the design more akin to that of the B factories. While the rf voltage required is low at 50 MV, we assume that it will be provided by the superconducting cavities required for operation at 200 GeV. The dynamic heat load and the HOM power generated in these cavities may be substantial at these high beam currents and may therefore rule out such a large beam current. Multibunch instabilities may also be severe and therefore require dedicated feedback systems for low energy operation. Finally the Sokolov-Ternov polarization time is 2600 h, thus physics with polarized beams is not an option at this energy unless one injects polarized beams into the ring.

In short, operation at 46 GeV will require several different challenges to be faced compared to operation at 200 GeV. It is not even clear if the components will be able to withstand the high beam currents required. Therefore, it makes more sense to consider a smaller ring for physics at the Z0 mass. A natural choice for this would be the injector to the large ring. Such a ring (a Z0 factory) was proposed by Keil [8].

TABLE VI. Select parameters of the 233 km ring operated as a collider at 46 GeV. The magnets are the same as at 200 GeV with parameters in Table I. The high beam current, large number of bunches, and long polarization time make this ring unsuitable for collider operation at 46 GeV.

Energy (GeV)	46.00
Luminosity	12.38×10^{33}
Synchrotron radiation power (both beams) (MW)	39.40
Number of bunches	46 600
Particles per bunch	1.47×10^{11}
Bunch current (mA)	0.0302
Emittances (nanometer)	16.59, 0.83
Beam-beam parameter	0.045
Single beam current (mA)	1408.08
Phase advance per cell (deg)	25.0
Dipole field (T)	0.005 78
Quad gradient (T/m)	1.161
rf voltage (GV)	0.05
Relative energy spread	0.239×10^{-3}
Bremsstrahlung lifetime (h)	168.9
Polarization time (h)	2600.8
Critical energy (keV)	6.514

TABLE VII. Parameters of a 46 GeV ring that would fit on the site of Fermilab and serve both as an injector to the VLLC and as a collider at the Z pole.

Circumference (km)	15.00
Energy (GeV)	46.000
Luminosity	5.16×10^{33}
Synchrotron radiation power (both beams) (MW)	60.8
Number of IPs	1
β_x^*, β_y^* (cm)	100.000, 1.000
σ_y^*, σ_y^* (μm)	231.744, 2.317
Number of bunches	74
Bunch spacing (km)	0.203
Bunch frequency (Mhz)	1.48
Particles per bunch	4.851×10^{11}
Bunch current (mA)	1.553
Emittances (nanometer)	53.705, 0.537
Single beam current (mA)	114.94
Arc radius (m)	1750.0
Bend radius (m)	1500.0
Number of cells	162
Phase advance per cell (deg)	90.0
Length of cell (m)	67.52
Dipole field (T)	0.1023
Quad gradient (T/m)	20.0
Quadrupole length (m)	0.321
Cell $\sigma_x^{\max}, \sigma_y^{\max}$ (mm)	2.488, 0.249
Max apertures required (cm)	4.067, 1.249
Max and min dispersion (m)	1.763, 0.842
Momentum compaction	0.546×10^{-3}
Harmonic number	20 014
Energy loss per turn (GeV)	0.265
Damping time (turns)	173
rf voltage (GV)	0.408
Relative energy spread	0.102×10^{-2}
Synchrotron tune	0.1084
Bunch length (mm)	12.231
Longitudinal emittance (eV sec)	0.006
Bremsstrahlung lifetime (h)	5.99
Polarization lifetime (h)	0.45
Critical energy (keV)	123.39
Number of photons/m/sec	0.453×10^{18}
Linear power load (single beam) (kW/m)	2.76

We consider a similar ring here but with a circumference chosen to be 15 km. This would just fit within the Fermilab site. This choice is motivated by discussions at the Snowmass 2001 Conference where it was pointed out that the tunnel for this "site filler" could also be used for a 5 TeV proton injector to a VLHC. Unlike the design proposed by Keil [8], we choose not to use polarization wigglers. Electrons and positrons into this machine are delivered from the main injector (MI) at an energy of 12 GeV. As a design strategy we choose the bunch intensity in this 46 GeV machine to be the same as in the VLLC. If we assume that the transverse impedance per unit length is the same in the two machines, the bunch intensity should be safely below the TMCI threshold at energies in the range from 12–46 GeV, assuming that the impedance model ensures that we are below the TMCI threshold by a factor of 2 in the VLLC. Another advantage of this choice of bunch intensity is that, if the optimal filling cycle for the VLLC requires that bunches be injected at full intensity into the VLLC and immediately accelerated to top energy, the filling cycle for the 46 GeV synchrotron is the same whether it is used as an injector or as a Z factory.

Table VII shows the parameters of this injector ring at the top energy of 46 GeV. The luminosity is just above 5×10^{33} cm^{-2} sec^{-1} which with standard assumptions on operation times amounts to about 10^9 Z events a year. The bunch frequency is 1.5 MHz, a number small enough that the detector will not be saturated with too many Z events per second [34]. The polarization time is reasonable at 27 min. The dipole field is close to that of the fields of the LEP dipoles. Overall the parameters of this ring appear reasonable for use as a Giga-Z factory.

IX. SCALING LAWS WITH ENERGY AND RADIUS

In the previous two sections we developed parameter sets for operation at 200 and 46 GeV, respectively. The design philosophies at these two energies were quite different. The main interest in this ring, however, is at the high energy end so it is important to determine the useful upper limit in energy for this machine. Thus for all energies above approximately 100 GeV, the design philosophy outlined in Sec. II is relevant.

We assume that magnet lengths and phase advances are chosen at some energy of interest and kept fixed thereafter. Table VIII shows the scaling with energy of some of the important parameters. Most of these dependences on energy are well known. For example, the equilibrium emittance increases as γ^2 and the rf voltage increases as γ^4. The additional twist here is that the beam-beam parameter is allowed to scale with energy and recent data (see Sec. IV) suggest that in a given machine $\xi_y^{\max} \sim \gamma^{1.2}$. If we are to operate at the beam-beam limit at all energies, then (i) the luminosity drops much more slowly with energy $\gamma^{-1.8}$ compared to γ^{-3} without the scaling of the beam-beam parameter and (ii) the bunch intensity increases more rapidly as $N_b \sim \gamma^{4.2}$ rather than γ^3. The e^+-e^- bremsstrahlung lifetime also drops faster with energy as $\tau_L \sim \gamma^{-2.2}$ in this scenario.

TABLE VIII. Scaling of beam parameters with energy. Machine circumferences and synchrotron radiation power are kept fixed.

Parameter	Energy dependence
Equilibrium emittance ϵ_x	γ^2
Energy loss U_0, rf voltage $V_{\rm rf}$	γ^4
Damping time $\tau_s \sim E/U_0$	γ^{-3}
Maximum beam-beam parameter $\xi_y \sim \tau_s^{-0.4}$	$\gamma^{1.2}$
Luminosity $\mathcal{L} \sim \xi_y \gamma^{-3}$	$\gamma^{-1.8}$
Bunch intensity $N_b \sim \xi_y \gamma \epsilon_x$	$\gamma^{4.2}$
Maximum number of bunches $M_B^{\max} \sim 1/N_b E^4$	$\gamma^{-8.2}$
Synchrotron frequency ν_s	$\gamma^{3/2}$
Equilibrium energy spread σ_E/E	γ
Bunch length σ_s	$\gamma^{-1/2}$
Critical energy E_c	γ^3
Bremsstrahlung lifetime $\tau_L \sim 1/\xi_y \gamma$	$\gamma^{-2.2}$

Figure 8 shows the values of luminosity and rf voltage as a function of energy with a ring circumference of 233 km and synchrotron radiation power kept constant at 100 MW. As mentioned above, ξ is allowed to scale with energy and the values at some of the energies are shown in the figure. We observe that, if a maximum of 12 GV of rf is available, the energy reach of a single beam in this ring extends from 100 to 250 GeV with luminosities in the range from $0.6–3 \times 10^{34}$ cm^{-2} sec^{-1}. A complete list of parameters at other energies may be found on the World Wide Web [35].

If this collider is to be part of a staged approach to a large tunnel housing both lepton and hadron accelerators which will be upgraded in energy and/or luminosity over time, it makes sense to consider how the lepton collider

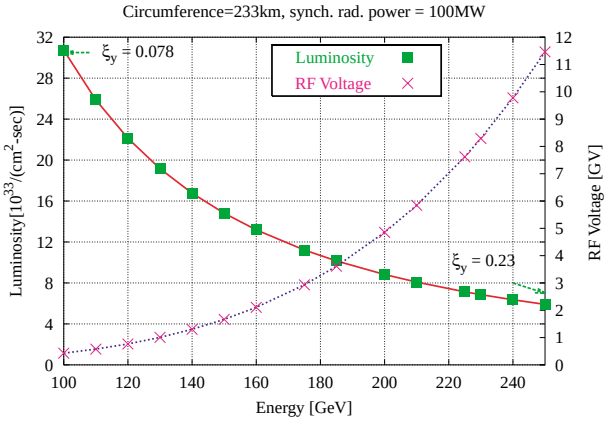

FIG. 8. (Color) Achievable luminosities and the rf voltages required as a function of energy at a ring circumference of 233 km. The synchrotron radiation power is kept constant at 100 MW for energies at and above 100 GeV. The beam-beam parameter scales with the damping decrement as discussed in Sec. IV.

TABLE IX. Scaling of beam parameters with the bend radius ρ. Luminosity and synchrotron radiation power are kept fixed.

Parameter	Radius dependence
Maximum energy E	$\rho^{1/3}$
Equilibrium emittance $\epsilon_x \sim \gamma^2/R^3$	$\rho^{-7/3}$
Bunch intensity $N_b \sim \xi_y \gamma \epsilon_x$	ρ^{-2}
Maximum number of bunches $M_B^{\max} \sim \rho/f_{\rm rev} N_b \gamma^4$	$\rho^{8/3}$
rf voltage $V_{\rm rf} \sim \gamma^4/\rho$	$\rho^{1/3} \sim \gamma$
Relative energy spread $\sigma_E/E \sim \gamma/\sqrt{\rho}$	$\rho^{-1/6}$
Synchrotron frequency $\nu_s \sim \sqrt{hV_{\rm rf}\eta/E}$	$\rho^{1/2}$
Bunch length $\sigma_s \sim 1/\omega_s(\sigma_E/E)$	$\rho^{1/3}$
Critical energy $E_c \sim \gamma^3/\rho$	const
Damping time $\tau_s \sim E^3/\rho$	const
Maximum beam-beam parameter $\xi \sim \tau_s^{-0.4}$	const
Bremsstrahlung lifetime $\tau_L \sim 1/f_{\rm rev}\gamma$	$\rho^{2/3}$

parameters scale with the machine radius. This would help determine an optimum radius. Once the parameters are determined at one circumference, the scaling laws may be used to calculate the parameters at any other circumference. Table IX shows the scaling with radius of some of the important parameters.

Some comments on these scalings are in order. Because of the strong dependence of the emittance on the focusing in the arcs, the emittance actually *decreases* with machine radius even though the energy has increased. The bunch intensity also decreases with increasing radii and faster than the emittance in order to keep the beam-beam tune shift constant. The number of bunches must be increased to avail the maximum rf power when the machine radius is increased. $V_{\rm rf}$ and maximum energy both increase with the cube root of the machine radius. The critical energy, the damping time measured in turns, and therefore the damping decrement λ_d and maximum beam-beam parameter ξ_y do not change with machine size.

X. AN INJECTOR SYSTEM

The Fermilab accelerator complex (linac, Booster, and Main Injector) could be used as the basis for an e^+e^- injector if the beam energies were somewhat reduced from those used for protons. The specifications of an injector system could follow the design of the LEP [36] and HERA [37] injectors or the APS [38] injection system.

Two new electron linacs would be required. The first would operate at about 3 GHz and accelerate electrons to an energy of around 200 MeV, which would be sufficient to produce positrons. A positron production target would be followed by a second linac section to produce a positron energy high enough to inject into the positron damping ring. Since the positrons will be produced at a much lower flux and larger emittance than electrons, it is necessary to damp and collect positrons from many pulses before further acceleration. The CERN, HERA, and APS damping rings are very compact and operate at energies of around 400–600 MeV. The operation of these systems in the same enclosure, parallel to the Fermilab proton linac, seems possible, During the checkout of the FNAL 805 MHz linac upgrade, the linac tunnel was operated essentially with two parallel linacs, so the addition of a e^+e^- linac line would not crowd the existing facility [39].

We have considered the use of the FNAL Booster to accelerate the e^+ and e^- to higher energies; however, the use of gradient magnets in the lattice makes this ring somewhat inappropriate for electrons, since this lattice affects the damping partition numbers in undesirable ways. In order to eliminate this problem, a correction package, consisting of a gradient magnet and a quadrupole, should be inserted into the ring to correct the damping partition numbers. The Booster has sufficient space to accommodate this package. Similar packages have been used in the Proton Synchrotron at CERN.

It is unclear if it is more efficient to reverse the magnetic field in the accelerator structures or build injection lines so beams could circulate in opposite directions. We assume the fields will not be reversed and injection and extraction systems would have to be added to the Booster for e^+e^- operation. The maximum energy that could be reached with the existing rf would be around 3 GeV. Since a new proton source is being considered for a neutrino source and muon collider, which would not fit in the existing Booster tunnel, there is also the possibility of designing a compact, separated function magnet lattice to replace the existing Booster magnets.

We assume electrons and positrons would be injected into the Main Injector in opposite directions at an energy of around 3 GeV. This energy would require the MI magnets to operate at a much lower field than would ever be used for protons; however, the magnets have been measured at this low field and the field quality seems to be acceptable for electron operation [40]. The maximum energy that could be produced in the Main Injector is around 12 GeV, due to the limited rf and the limited space for adding more. The beams would then be extracted in opposite directions into the VLHC Booster tunnel for acceleration up to the injection energy of the VLHC ring.

A third synchrotron is probably required since the 12 GeV electrons from the MI injected into the collider ring would require the average magnetic field to be about 16 G, which should be compared to the 215 G injection field of LEP. We have studied the properties of an electron ring in the tunnel of a low field VLHC Booster in the context of an electron-proton collider [41]. Such a ring could have a maximum energy up to about 80 GeV with an installed rf voltage of 1.09 GV. We assume this rf operates at 352 MHz. If the VLHC Booster ring was used only as an injector, an injection energy of around 40 GeV could be accommodated with an rf voltage of about 60 MV.

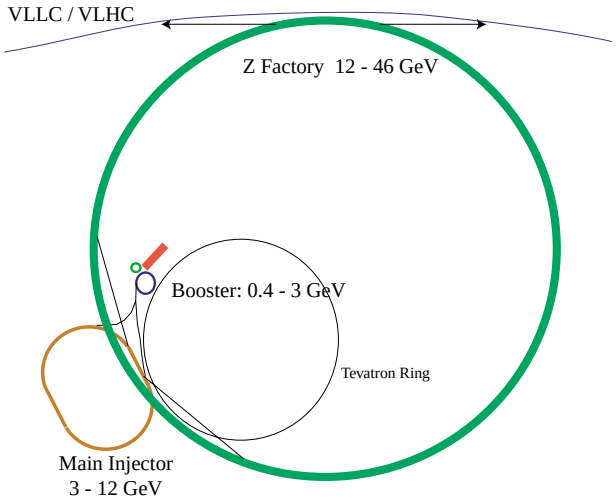

FIG. 9. (Color) Layout of the injectors for the VLLC and the VLHC. The tunnel housing the Z factory is 15 km around and fits within the Fermilab site. It could also be used to house an injector for the VLHC [42].

The alternative suggestion by Keil [8] of building an injector with a beam energy of 46 GeV, discussed in Sec. VIII, has a number of desirable results. A higher energy injector makes injection into the high energy ring easier, and raises the transverse mode coupling instability threshold, permitting more intense bunches. In addition, the injector is at an energy where it could be carefully optimized for operation as a Giga Z Factory, with bunches circulating in a comparatively small ring. This permits staging in that the injector can be producing useful physics while the large ring is under construction. When the facility is complete, there would be the opportunity of using the injector for Z^0 physics while the high ring is used for Higgs, SUSY, and top quark physics. Figure 9 shows the schematic layout of the injectors together with their energy range.

Operational cycle

The operational cycle will need to be optimized to minimize the filling time and maximize the integrated luminosity in the collider. The details of the filling cycle depend on a number of parameters that are unknown at this stage, such as the number of electrons/positrons per pulse from the linacs, the damping time in the modified Booster, etc. Nevertheless, with some assumptions we can outline a sketch of a filling procedure. Table X shows some relevant parameters of the injector synchrotrons and the collider. The ratio of circumferences of these machines is 1:7:4.52:15.53. If we assume for the moment that each bunch can be filled to the required intensity by single turn injection into each synchrotron, a bunch current of 0.1 mA in the VLLC corresponds to bunch currents of 1.55 mA in the Z factory, 7 mA in the Main Injector, and 49 mA

TABLE X. Relevant injector parameters for the operational cycle.

	Booster	Main Injector	Z factory	VLLC
Circumference (km)	0.474	3.319	15.0	233.0
Injection energy (GeV)	0.4–0.6	3	12	46
Harmonic number	84	588	20 014	273 576

in the Booster. Space charge effects, synchrotron radiation doses, to name but a few effects, rule out such high currents in the Booster. Thus several Booster cycles are required which must also provide for transmission losses in the injector chain. In each Booster cycle, a maximum of 82 bunches can be extracted to the Main Injector. At 200 GeV, 114 bunches are required in the VLLC to obtain the maximum luminosity while respecting the synchrotron power limit of 100 MW. One possibility is to extract these bunches in two Booster batches, with an equal number of bunches in each batch, to the Main Injector. If the cycle time is roughly the same as it is at present, which accelerates protons from 400 MeV to 8 GeV, a batch can be delivered at an energy of 3 GeV to the Main Injector every 1.5 sec or less. For Tevatron collider operation, the Main Injector operates on a 4 sec cycle accelerating protons from 8 to 150 GeV. This includes 1.45 sec during flattop at injection energy when proton bunches are coalesced and cogged. With e^+e^- operation, the Main Injector would accelerate particles from 3 to 12 GeV, perhaps in a single batch of 114 bunches and without accumulation of intensities. Particles could be extracted in a single turn to the Z factory which in turn accelerates them to 46 GeV where they are extracted to the VLLC. In the collider, damping times are short and these freshly injected bunches could coalesce with the circulating beam. In this scenario, bunch intensities are accumulated only in the collider. Another, perhaps more promising, option is to accumulate bunches to full intensity in the 46 GeV synchrotron where the damping time is also relatively short. This has the advantage that in the VLLC bunches can be accelerated immediately after injection and so minimize the time spent at injection energy when instabilities are the most dangerous. However, detailed studies are required, and other scenarios where accumulation takes place in the other injector synchrotrons as well may be more optimal.

XI. TECHNOLOGICAL CHALLENGES

The primary technical challenges seem to be cooling the vacuum chamber, disposing of the heat produced, and determining how low the field of the collider magnets can be confidently run, since this minimum field determines the design of the magnets and the injection energy. In addition, however, there are a number of other technical problems which must be considered.

A. Vacuum system

In addition to the usual synchrotron radiation induced gas desorption, the vacuum chamber design is determined by a number of constraints. Although the power density of the synchrotron radiation deposition is smaller than at many other storage rings and synchrotron sources, the critical energy of the synchrotron photons spans a large range (5–500 keV), and the large bend radius complicates the power deposition. In addition, the large circumference requires a design which both minimizes beam wall interactions and is inexpensive.

The large range in critical energy of the synchrotron radiation implies that the power in *low* energy beams will be deposited mostly inside the vacuum chamber, but the chamber will become transparent to *high* energy photons, so external absorbers are required for high energies. The high energy photons will also be subject to internal reflection at grazing incidence, but are poorly attenuated by aluminum. These photons are a radiation hazard to electronics and cable insulation, thus the absorbers must be shielded to ensure useful radiation levels in the tunnel.

The large bending radius complicates even deposition of synchrotron radiation power on the vacuum chamber walls since these chambers would be expected to move slightly with operational temperature fluctuations and the motion of the earth. Since deposition on the wall is not expected to be constant, we assume that the vacuum chamber would have an antechamber that would conduct the synchrotron radiation to lumped absorber/window assemblies where the power could be absorbed and the synchrotron radiation outgassing could be pumped.

In order to minimize both the beam-wall interactions and the cost and complexity of the vacuum system, it may be desirable to use prebaked chambers and weld the aluminum vacuum sections *in situ* without a subsequent bakeout [43]. This makes assembly easier, eliminates the need for bellows with a large mechanical range, reduces the rf loss factor induced by the bellows on the beam (both due to the number and complexity of bellows), and reduces the cost and complexity of the vacuum system as a whole. Since the chamber will heat up somewhat during normal operation, some bellows are required. It is, however, highly desirable to avoid the expansion involved in a high temperature bake ($\Delta l = \alpha l \Delta T = 2.4 \times 10^{-5} \times 100 \times 100 = 24$ cm) for lengths l and ΔT of 100 m and 100 °C. In order to do this, one must have sufficient pumping in the chamber to ensure that a pressure of 10^{-8} Torr can be achieved, which would allow a beam lifetime of about 1 h and permit subsequent wall scrubbing by synchrotron radiation.

B. Cooling system

The warm water produced in the synchrotron absorbers is also a concern. Since there will be roughly 100 MW of heating, distributed over 230 km, we assume this heat must be brought to the surface where cooling towers would be used to discharge it into the atmosphere. This system would be a significant environmental perturbation on the surface. We have also looked at discharging the heat into the ground and into surface water. Since the tolerable thermal range of the system is fairly narrow, due to the fact that thermal expansion must be minimized, the temperature range of the water would also be comparatively limited, thus it would be difficult to recover any useful power from the waste water.

C. Magnet design

The primary issue with the injector system design is determining the minimum field where the ring magnets can usefully transport beam. Since the bending magnets in the arcs operate at a field of B_{inj} [G] $= 1.3E$ [GeV], and the error fields at injection should be below $(10^{-4}-10^{-3})B_{\mathrm{inj}}$, error fields due to external sources, other components, and remanent fields, could be a problem. A final injector synchrotron must then be designed which can produce beams in the required energy. This synchrotron can be located in the tunnels which would be eventually occupied by the hadron Booster.

We have shown that external fields can be well attenuated by the magnet yoke itself and extensive shielding of magnets may not be required [44,45]. The remanent fields at low excitation are a function of the specific alloy used, and a number of alloys exist with very low remanent fields; however, their costs tend to be higher than steel. One option seems to be the use of vacuum or hydrogen annealed steel [46]. This anneal removes carbon from the steel very efficiently, reducing the remanent field and hysteresis loses by a significant factor, as shown in Fig. 10 [47]. It seems as though an order of magnitude reduction in remanent fields

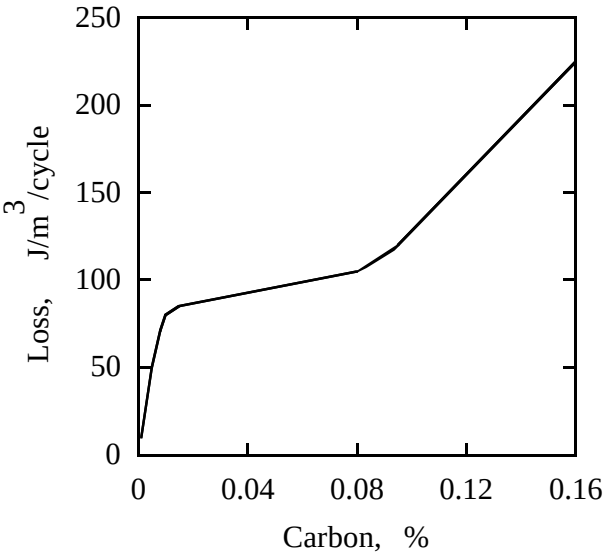

FIG. 10. Hysteresis loss as a function of carbon content in steel.

from the standard low carbon 1010 alloy (~0.1% carbon) may be possible in an alloy which is not significantly more expensive than standard commercially produced ones.

D. Other components

A number of other systems and design issues have not been considered in any significant detail in this paper. We assume that superconducting rf cavities will be necessary. The design of these cavities must suppress higher order modes efficiently.

It is not clear if the e^+-e^- collider arcs would be optimized with one or two rings. While it is possible to assume that pretzel orbits can be produced in the comparatively long arcs, it is not clear if parasitic collisions will produce significant emittance growth to justify the construction of a second set of arc magnets. This may significantly affect the cost.

The placement of the rf cavities will determine the energy of the beam around the ring. Since so much energy is added per turn, it may be necessary to distribute the cavities around the ring. This might require zero dispersion straights at a number of locations.

If the e^+-e^- collider and the low field hadron collider magnets are energized at the same time, the lepton collider will need to be protected from the fringe fields of the hadron collider. These fringe fields at a distance of about a meter are of the order of a few hundred Gauss, about the same level as the main bending field in the lepton collider.

Extensive masking and collimation systems will be required to protect the detector components from synchrotron radiation.

XII. CONCLUSIONS

We have explored the feasibility of a large electron-positron collider within the context of a staged approach to building a very large hadron collider. We have shown that in a ring of circumference 233 km, a lepton collider with $200 \leq E_{\rm cm} \leq 500$ GeV with synchrotron radiation power limited to 100 MW would require rf voltages comparable to LEP and would achieve luminosities in the range $(0.6-3) \times 10^{34}$ cm^{-2} sec^{-1} with reasonable choices of beam parameters. The achievable energy extends to nearly 1000 GeV (center of mass) at a lower luminosity of 10^{33} cm^{-2} sec^{-1}, but an unrealistic rf voltage is required to replenish the energy lost by the beam.

Such a machine derives benefits from its size and operating energy in that the limiting beam-beam tune shifts may be much higher than even those seen at LEP. In addition, it may be possible to further optimize the operation of this machine, particularly the interaction regions, to operate with a smaller β_y^* than was used in LEP. A preliminary IR design [13] shows that $\beta_y^* = 1$ cm may be feasible. There are a number of open issues which require more effort. It is not clear what the upper limit on ξ_y is, nor what the maximum number of bunches in the ring are. The demand for collisions prevented significant experimental work at LEP on these issues, but they can be studied theoretically. There may be ways of overcoming the TMCI limitations by coalescing electron bunches at high energies, but this has never been done. There are also some other questions. Is feedback useful against TMCI? What does an optimized 46 GeV Z0 factory look like? How can polarization at high energies be optimized? Would one ring suffice for the large ring or are two rings necessary? What is the optimum method of pumping the long vacuum chamber sections? How much cost and power minimization is possible in the complete design? These questions will require continuing study and experimental work.

One of the conclusions of the hadron collider working group at the Snowmass 2001 Conference was that the lattice design of this e^+e^- collider is compatible with the VLHC [42]. The decision on whether to build a lepton collider in a tunnel housing a very large hadron collider must ultimately be based on the physics reach at these energies. Assuming that the physics case is compelling, the design of such an accelerator can proceed to the next stage. The cost of the technical components in the lepton collider will likely be dominated by the superconducting rf cavities and the vacuum system. Improvements in design and technology can be expected to reduce the cost a decade from now compared to what they are today. Several technical challenges have to be faced but none appear to be insurmountable.

ACKNOWLEDGMENTS

We thank Ernie Malamud for initiating this study, Alvin Tollestrup for his encouragement, Mike Syphers and Steve Peggs for their interest. We acknowledge useful suggestions and comments by Eberhard Keil, Oswald Grobner, Ralph Assmann, and Karel Cornelis of CERN, Gerry Dugan and Richard Talman of Cornell, Desmond Barber of DESY, Lee Teng and Sushil Sharma of Argonne, and Uli Wienands from SLAC. This work was funded by DOE through Contracts No. DE-AC02-76CH03000 to Fermilab and No. W-31-109-ENG-38 to Argonne National Laboratory. The workshop held at IIT [3] was funded by the Illinois Consortium for Accelerator Research (ICAR).

APPENDIX A: USEFUL FORMULAS

Unless specified otherwise, the formulas in this section are obtained from the article by Sands [48].

Luminosity:

$$\mathcal{L} = \frac{N_{e^+} N_{e^-} M_b f_{\rm rev}}{4\pi} \frac{1}{\sqrt{\beta^*_{x,e}\epsilon_{x,e}}\sqrt{\beta^*_{y,e}\epsilon_{y,e}}}, \qquad \text{(A1)}$$

where N_{e^+}, N_{e^-} are the bunch intensities, M_b is the number of bunches.

Equilibrium horizontal emittance:

$$\epsilon_x = \frac{C_q \gamma^2}{J_x} \left[\frac{\oint \mathcal{H}/\rho^3 \, ds}{\oint 1/\rho^2 \, ds} \right]. \tag{A2}$$

The equilibrium emittance in a lattice built entirely with FODO cells scales with the horizontal phase advance μ_x^C per FODO cell as [49]

$$\epsilon_x(\mu_x^C) = 4 \frac{C_q \gamma^2}{J_x} \theta^3 \times \frac{1 - \frac{3}{4}\sin^2(\mu_x^C/2) + \frac{1}{60}\sin^4(\mu_x^C/2)}{\sin^2(\mu_x^C/2)\sin\mu_x^C}, \tag{A3}$$

where $C_q = (55/32\sqrt{3})\hbar/mc = 3.84 \times 10^{-13}$ m, J_x is the horizontal damping partition number, and θ is the bending angle in half of the FODO cell.

Momentum compaction:

$$\alpha_C \approx \frac{L_{\rm arc}}{C} \frac{\theta^2}{\sin^2(\mu_c/2)}, \tag{A4}$$

where $L_{\rm arc}, C$ are the lengths of the arcs and the circumference, respectively, θ is the bend angle per half cell, and μ_c is the phase advance per cell.

Energy equilibrium spread:

$$\frac{\sigma_E}{E} \approx \sqrt{\frac{C_q}{J_s \rho}} \gamma, \tag{A5}$$

where

$$C_q = \frac{55}{32\sqrt{3}} \frac{\hbar c}{mc^2} = 3.84 \times 10^{-13} \text{ m}$$

for electrons and positrons. J_s is the longitudinal damping partition number and ρ is the bending radius.

Equilibrium bunch length:

$$\sigma_s = \frac{c\,|\,\eta\,|}{\omega_s} \frac{\sigma_E}{E} = \frac{c}{\sqrt{2\pi} f_{\rm rev}} \sqrt{\frac{|\,\eta\,|E}{heV_{\rm rf}\cos\psi_s}} \frac{\sigma_E}{E}, \tag{A6}$$

where η is the slip factor, ω_s is the angular synchrotron frequency, and the other symbols have their usual meanings.

Energy acceptance:

$$\left(\frac{\Delta E}{E}\right)_{\rm accept} = \sqrt{\frac{eV_{\rm rf}}{\pi h|\eta|E} G(\phi_s)}, \qquad G(\phi_s) = 2\cos\phi_s - (\pi - 2\phi_s)\sin\phi_s. \tag{A7}$$

Beam-beam tune shifts:

$$\xi_x = \frac{N_b r_e \beta_x^*}{2\pi\gamma\sigma_x^*(\sigma_x^* + \sigma_y^*)}, \qquad \xi_y = \frac{N_b r_e \beta_y^*}{2\pi\gamma\sigma_y^*(\sigma_x^* + \sigma_y^*)}. \tag{A8}$$

In the limit $\sigma_x^* \gg \sigma_y^*$,

$$\xi_x = \frac{N_b r_e \beta_x^*}{2\pi\gamma(\sigma_x^*)^2}, \qquad \xi_y = \frac{N_b r_e \beta_y^*}{2\pi\gamma\sigma_x^*\sigma_y^*}. \tag{A9}$$

Energy lost by electrons per turn:

$$U = C_\gamma \frac{E^4}{\rho}, \qquad C_\gamma = \frac{4\pi}{3} \frac{r_e}{(m_e c^2)^3} = 8.86 \times 10^{-5} \text{ m/GeV}^3. \tag{A10}$$

Synchrotron radiation power in beam:

$$P_{\rm synch} = \frac{UI_e}{e}. \tag{A11}$$

Critical energy [50]:

$$E_{\rm crit}\ [\text{keV}] = 2.218 \frac{E^3\ [\text{GeV}]}{\rho\ [\text{m}]}. \tag{A12}$$

Critical wavelength [50]:

$$\lambda_{\rm crit}\ [\text{Å}] = \frac{4\pi\rho}{3\gamma^3} \times 10^{10}. \tag{A13}$$

Number of photons emitted per second by a particle:

$$N_\gamma = \frac{15.0\sqrt{3}}{8.0} \frac{P_{\rm synch}\ [\text{MW}]}{eN_b E_{\rm crit}\ [\text{keV}}] \times 10^3. \tag{A14}$$

Total photon flux [51]:

$$\dot{N}_\gamma\ [\text{photons/sec}] = 8.08 \times 10^{17} \times I\ [\text{mA}] E\ [\text{GeV}]. \tag{A15}$$

Gas load [51]:

$$Q_\gamma\ [\text{Torr} - \text{liters}\,\text{m}^{-1}\,\text{sec}^{-1}] = 4.5 \times 10^{-20} \eta_{\rm photo} \phi_\gamma, \tag{A16}$$

where $\eta_{\rm photo}$ is the photodesorption coefficient and $\phi_\gamma = \dot{N}_\gamma / L_{\rm arc}$ is the photon flux per unit length.

Damping partition numbers:

$$J_s \simeq 2.0, \qquad J_x + J_y + J_s = 4. \tag{A17}$$

For a FODO cell in the thin-lens approximation,

$$\frac{dJ_x}{d\delta} = -4 \frac{L_D}{L_Q} \left[\frac{2 + \frac{1}{2}\sin^2\mu/2}{\sin^2\mu/2} \right]. \tag{A18}$$

Damping times:

$$\tau_0 = \frac{E}{f_{\rm rev} U}, \qquad \tau_s = \frac{2}{2 + \mathcal{D}} \tau_0 \approx \tau_0, \qquad \tau_y = 2\tau_0, \qquad \tau_x = \frac{2}{1 - \mathcal{D}} \tau_0 \approx \tau_y, \tag{A19}$$

$$\mathcal{D} = \frac{\langle \frac{D}{\rho^2}(\frac{1}{\rho} + 2\frac{B'}{B})\rangle}{\langle \frac{1}{\rho^2}\rangle}. \tag{A20}$$

Longitudinal quantum lifetime:

$$\tau_{\mathrm{quant};s} = \frac{\tau_s}{N_{\mathrm{QL}}^2} \exp\left[\frac{1}{2} N_{\mathrm{QL}}^2\right], \qquad N_{\mathrm{QL}} = \left(\frac{\Delta E_{\mathrm{rf}}}{\sigma_E}\right), \tag{A21}$$

where ΔE_{rf} is the energy acceptance of the bucket provided by the rf system, σ_E is the sigma of the energy distribution, and τ_s is the longitudinal synchrotron radiation damping time. This is the expression due to Sands [48], but there are other (perhaps more accurate) expressions.

Transverse quantum lifetime:

$$\tau_{\mathrm{quant};\beta} = \frac{e^{r_\beta}}{2r_\beta}\tau_\perp, \qquad r_\beta = \frac{1}{2}\left(\frac{x_{\mathrm{apert},\beta}}{\sigma_\beta}\right)^2, \tag{A22}$$

where $x_{\mathrm{apert},\beta}$ is the transverse position of the aperture limitation, σ_β is the transverse sigma of the particle distribution, and $t_{\mathrm{damp},\perp}$ is the transverse synchrotron radiation damping time. If there is finite dispersion at the location of the aperture limitation, Chao's formula [52] holds,

$$\tau_{\mathrm{quant};\beta} = \frac{1}{\sqrt{2\pi}} \frac{\exp[r_{\beta,\delta}]}{(2r_{\beta,\delta})^{3/2}} \frac{1}{(1+f)\sqrt{f(1-f)}}\tau_\perp, \tag{A23}$$

where

$$r_{\beta,\delta} = \frac{1}{2}\left(\frac{x_{\mathrm{apert},\beta}}{\sigma_T}\right)^2, \qquad \sigma_T^2 = \sigma_x^2 + D_x^2\sigma_\delta^2,$$

$$f = \frac{D_x^2\sigma_\delta^2}{\sigma_T^2},$$

where D_x is the dispersion at the location of the aperture and σ_δ is the relative momentum deviation. For a fixed transverse damping time, the quantum lifetime depends on the parameters $f, r_{\beta,\delta}$ and has minimas at specific values of these parameters.

e^+e^- bremsstrahlung cross section: The dominant process that determines the lifetime at collision is small angle forward radiative Bhabha scattering which has a cross section given by [53]

$$\sigma_{e^+e^-} = \frac{16}{3}\alpha r_e^2\left\{-\left[\ln\left(\frac{\Delta E}{E}\right)_{\mathrm{accept}} + \frac{5}{8}\right] \times \left[\ln(4\gamma_{e^+}\gamma_{e^-}) - \frac{1}{2}\right] + \frac{1}{2}\ln^2\left(\frac{\Delta E}{E}\right)_{\mathrm{accept}} - \frac{\pi^2}{6} - \frac{3}{8}\right\}, \tag{A24}$$

where $(\Delta E/E)_{\mathrm{accept}}$ is the rf acceptance of the bucket. Definitions of symbols used in this paper are given in Table XI.

TABLE XI. Definitions of symbols.

c	Velocity of light
e	Electron charge
E	Beam energy
f_{rev}	Revolution frequency
h	Harmonic number
$\mathcal{H}$	Lattice factor $= [\eta^2 + (\beta\eta' - \beta'\eta/2)^2]/\beta$
I_b	Bunch current
I	Beam current in a single beam
J_x, J_y, J_s	Horizontal and longitudinal partition numbers
$k_\perp, k_\parallel$	Transverse, longitudinal loss factor
$\mathcal{L}$	Luminosity
m_e	Electron mass
M_b	Number of bunches in the ring
N_b	Number of particles in a bunch
P_T	Synchrotron power lost in both beams
r_e	Classical electron radius
R	Arc radius
V_{rf}	Maximum rf voltage
α_c	Momentum compaction
β_x, β_y	Beta function at some point in the ring
β_x^*, β_y^*	Beta function at the interaction point
γ	Relativistic factor
δ	Momentum variation
ϵ_x, ϵ_x	Horizontal, vertical emittance
η	Slip factor
κ	Emittance ratio $= \epsilon_y/\epsilon_y$
λ_d	Damping decrement
μ_x, μ_y	Phase advance per cell
ν_s	Synchrotron tune
ν_x, ν_y	Arc tunes
ξ_x, ξ_y	Beam-beam tune shift
ρ	Bending radius
σ_x, σ_y	Beam radius
σ_E	Bunch energy spread
σ_x^*, σ_x^*	Beam radius at interaction point
τ_L	Beam lifetime
ϕ_s	Synchrotron phase

APPENDIX B: SCALING OF THE BEAM-BEAM PARAMETER

Consider a simple model of the beam-beam kicks that treats them as random kicks similar to those due to photon emission. This model should become more accurate as the radiation damping time decreases so that kicks from turn to turn become more uncorrelated. We follow Sands' notation here.

In the linearized approximation of the beam-beam kicks,

$$\Delta x' = -\frac{2N_b r_e x}{\gamma\sigma_x^*(\sigma_x^* + \sigma_y^*)}. \tag{B1}$$

The change in amplitude $a_x^2 = [x^2 + (\beta_x x' + \alpha_x x)^2]/\beta_x$ due to a beam-beam kick is

$$\Delta a_x^2 = 2(\beta_x x' + \alpha_x x)\Delta x' + \beta_x(\Delta x')^2. \tag{B2}$$

At the IP, $\alpha_x = 0$. So

$$x^* = \sqrt{\beta_x^*}\, a_x \cos\phi_x, \qquad x'^* = -\frac{a_x}{\sqrt{\beta_x^*}}\sin\phi_x. \tag{B3}$$

The beam sizes are assumed to stay matched at all stages so that $\sigma^*_{x,e^+} = \sigma^*_{x,e^-} = \sigma^*_x$ and $\sigma^*_{y,e^+} = \sigma^*_{y,e^-} = \sigma^*_y$. We assume that at high currents and large damping, the beam-beam kicks randomize the betatron phase from turn to turn. In this regime, nonlinear resonances are no longer very important. When we average the change in amplitude over all betatron phases, the term $\langle x'\Delta x'\rangle \sim \langle \sin\phi_x \cos\phi_x\rangle = 0$. If there are $N_{\rm IP}$ IPs, kicks from each of these are also considered as uncorrelated so that the net change in the squared amplitude is the sum of all these kicks,

$$\langle \Delta a_x^2\rangle_{N_{\rm IP}} = 2N_{\rm IP}\left(\frac{N_b r_e}{\gamma\sigma^*_x(\sigma^*_x + \sigma^*_y)}\right)^2(\beta^*_x a_x)^2. \quad \text{(B4)}$$

The rate of change of a_x^2 including the effects of random photon emissions and radiation damping is

$$\frac{d}{dt}\langle \Delta a_x^2\rangle_{N_{\rm IP}} = \mathcal{Q}_x - 2\frac{\langle a_x^2\rangle}{\tau_x} + \frac{\langle a_x^2\rangle}{\tau_1}, \quad \text{(B5)}$$

where

$$\mathcal{Q}_x = \frac{\langle N_\gamma \langle u^2\rangle \mathcal{H}\rangle_s}{E^2} \text{ (Sands' notation)}, \quad \text{(B6)}$$

$$\frac{1}{\tau_1} = 2\left(\frac{N_b r_e \beta^*_x}{\gamma\sigma^*_x(\sigma^*_x + \sigma^*_y)}\right)^2 N_{\rm IP} f_{\rm rev}. \quad \text{(B7)}$$

τ_1 defines a time scale for the beam-beam interactions. In the stationary state, the left-hand side of Eq. (B5) vanishes and $\langle a^2\rangle \equiv \langle a^2\rangle_{\rm eq} = 2\epsilon_{\rm eq}$, where $\epsilon_{\rm eq}$ is the equilibrium emittance. The beam sizes σ^*_x, σ^*_y at the IP are determined by the perturbed equilibrium emittances,

$$\sigma^{*2}_x = \beta^*_x \epsilon_{{\rm eq},x}, \qquad \sigma^{*2}_y = \beta^*_y \epsilon_{{\rm eq},y}. \quad \text{(B8)}$$

In the limit that $\sigma^*_x \gg \sigma^*_y$, assuming that this is still true after beam blow up in the vertical plane,

$$\frac{1}{\tau_1} = 2\left(\frac{N_b r_e \beta^*_x}{\gamma\sigma^{*2}_x}\right)^2 N_{\rm IP} f_{\rm rev} = 2\left(\frac{N_b r_e}{\gamma\epsilon_{\rm eq}}\right)^2 N_{\rm IP} f_{\rm rev}. \quad \text{(B9)}$$

Hence the equation for the equilibrium emittance is

$$\frac{1}{4}\mathcal{Q}_x = \frac{1}{\tau_x}\epsilon_{\rm eq} - \left(\frac{N_b r_e}{\gamma}\right)^2 N_{\rm IP} f_{\rm rev}\frac{1}{\epsilon_{\rm eq}}. \quad \text{(B10)}$$

In the absence of the beam-beam interactions, the equilibrium emittance is

$$\epsilon_0 = \frac{1}{4}\mathcal{Q}_x \tau_x. \quad \text{(B11)}$$

Solving the quadratic and keeping the positive root (the emittance increases with the beam current), we find

$$\epsilon_{\rm eq} = \frac{1}{2}\epsilon_0[1 + \sqrt{1 + 4\chi_{bb}}], \quad \text{(B12)}$$

where we have defined a dimensionless variable χ_{bb} as

$$\chi_{bb} = \left(\frac{N_b r_e}{\gamma}\right)^2 \frac{2}{\lambda_d \epsilon_0^2}. \quad \text{(B13)}$$

$\lambda_d = 1/(N_{\rm IP} f_{\rm rev}\tau_s) = 2/(N_{\rm IP} f_{\rm rev}\tau_x)$ is the damping decrement. We apply this to the LEP data with parameters given in Table I. The equilibrium emittance ϵ_0 in the absence of beam-beam effects is 21.3 nm. Using Eq. (B12), the equilibrium emittance with blowup due to the beam-beam is found to be 153 nm, an increase by more than a factor of 7. Measurements of the vertical emittance at LEP [17] showed that the emittance increased by roughly 50% at the highest currents compared to the values at low current. As is typical, the assumption of completely random uncorrelated beam-beam kicks overestimates their effect. The assumption that the entire betatron phase is random from turn to turn is a very strong one and likely to be wrong. A better starting point would be to assume that only part of the phase is random. A more sophisticated treatment with correlated random kicks is possible (for an example of diffusion due to beam-beam phenomena in hadron colliders see Ref. [54]). A Fokker-Planck treatment would be required for e^+-e^- beams, an analysis that we will leave to a future publication. Instead we will make an assumption that the effect of the partially random phases and correlated kicks can be described by a correction factor Γ so that

$$\epsilon_{\rm eq} = \frac{1}{2}\epsilon_0[1 + \sqrt{1 + 4\Gamma\chi_{bb}}]. \quad \text{(B14)}$$

Here $\Gamma < 1$ is to be treated as a dimensionless fit parameter which will not depend on the bunch intensity of the other beam but will depend on the tune, damping times, and the lattice configuration. This will suffice for our purpose here.

Consider the vertical beam-beam parameter

$$\xi_y = \frac{N_b r_r \beta^*_y}{2\pi\gamma\sigma^*_y(\sigma^*_x + \sigma^*_y)} \xrightarrow{\lim_{\sigma^*_x \gg \sigma^*_y}} = \frac{N_b r_r \beta^*_y}{2\pi\gamma\sigma^*_x\sigma^*_y}. \quad \text{(B15)}$$

In the presence of coupling parametrized by a ratio $\kappa = \epsilon_y/\epsilon_x$, the beam-beam parameter is

$$\xi_y = \frac{r_e(1+\kappa)}{2\pi\gamma}\sqrt{\frac{\beta^*_y}{\kappa\beta^*_x}}\frac{2N_b}{\epsilon_0[1 + \sqrt{1 + 4\Gamma\chi_{bb}}]} = \frac{2\xi_{y,0}}{[1 + \sqrt{1 + 4\Gamma\chi_{bb}}]}, \quad \text{(B16)}$$

where $\xi_{y,0}$ is the usual beam-beam parameter without the correction. When beam-beam effects are negligible, this reduces to the usual expression

$$\xi_y = \xi_{y,0} = \frac{r_e(1+\kappa)}{2\pi\gamma}\sqrt{\frac{\beta^*_y}{\kappa\beta^*_x}}\frac{N_b}{\epsilon_0}. \quad \text{(B17)}$$

At large beam currents $N_b \to \infty$, the N_b^2 term in χ_{bb} dominates the unperturbed emittance term so that the asymptotic limit is

$$\xi^\infty_y = \frac{\xi_{y,0}}{\sqrt{\Gamma\chi_{bb}}} = \frac{(1+\kappa)}{2\pi}\sqrt{\frac{\beta^*_y}{\kappa\beta^*_x}}\sqrt{\frac{\lambda_d}{2\Gamma}}. \quad \text{(B18)}$$

This is a lattice dependent constant, independent of current.

In the case of optimal coupling, $\epsilon_y/\epsilon_x = \beta_y^*/\beta_x^*$, which simplifies the above to

$$\xi_y^\infty = \frac{(1+\kappa)}{2\pi}\sqrt{\frac{\lambda_d}{2\Gamma}}.$$

This is clearly a very simple analysis, and many important details of the dynamics are missing. Some, such as the dynamic beta effect, are easily incorporated. A more severe limitation perhaps is the neglect of the nonlinearities of the beam-beam force. The resonance driving terms are probably not important in the extreme damping limit, but the purely action dependent terms in the beam-beam Hamiltonian can lead to important changes in the stability limit. These and other effects need to be considered in a more complete treatment.

[1] Second Annual VLHC Meeting, Port Jefferson, NY, 2000 (unpublished).

[2] C. Hill, in *Proceedings of the Workshop on an e^+e^- Storage Ring at the VLHC, Chicago, IL, 2001*, http://capp.iit.edu/capp/workshops/epem/ee_workshop_schedule.html.

[3] *Proceedings of the Workshop on an e^+e^- Collider in the VLHC Tunnel, Chicago, IL, 2001*, Fermilab Report No. Fermilab-Conf-01/107-T (http://fnalpubs.fnal.gov/archive/2001/conf/Conf-01-107-T.html).

[4] D. Brandt *et al.*, Rep. Prog. Phys. **63**, 939 (2000).

[5] A. Barcikowski, G. Goeppner, J. Norem, E. Rotela, B. Rusthoven, S. Sharma, L. Teng, K. Thompson, R. Assman, K. Cornelis, E. Keil, O. Groebner, S. Belomestnykh, G. Dugan, R. Talman, C. Johnstone, T. Sen, and A. Tollestrup, in Proceedings of the 2001 Particle Accelerator Conference, Chicago, IL, 2001 (to be published).

[6] T. Sen, J. Norem, S. Sharma, and L. Teng, in Proceedings of the 2001 Snowmass Workshop, Snowmass, CO (to be published).

[7] J. Gareyte, CERN Report No. CERN-SL-2000-075(AP), 2000.

[8] E. Keil in Ref. [3].

[9] G. Dugan, in Ref. [3].

[10] A. Burov *et al.*, Nucl. Instrum. Methods Phys. Res. Sect. A, **450**, 194 (2000).

[11] J. Jowett, in *Proceedings of the Fourth Workshop on LEP Performance, Chamonix, 1994,* edited by J. Poole, CERN Report No. CERN-SL/94-06, 1994, p. 47.

[12] E. Keil (personal communication).

[13] C. Johnstone and T. Sen, in Ref. [3].

[14] D. Brandt, W. Herr, M. Meddahi, and A. Verdier, in *Proceedings of the Particle Accelerator Conference, New York, 1999* (IEEE, Piscataway, NJ, 2000), p. 3005 (1999).

[15] E. Keil and R. Talman, Part. Accel. **14**, 109 (1983).

[16] S. Peggs, Workshop on the Effects of Synchrotron Radiation in the VLHC, BNL, 2000 (unpublished).

[17] R. Assmann and K. Cornelis, in *Proceedings of the European Particle Accelerator Conference, Vienna, 2000,* http://accelconf.web.cern.ch/AccelConf/e00/index.html, p. 1187.

[18] Ya. S. Derbenev and A. M. Kondratenko, Sov. Phys. JETP **37**, 968 (1973).

[19] D. Barber, in *Handbook of Accelerator Physics and Engineering,* edited by A. Chao and M. Tigner (World Scientific, Singapore, 1999).

[20] A. A. Sokolov and I. M. Ternov, Sov. Phys. Dokl. **8**, 1203 (1964).

[21] J. Buon and J. P. Koutchouk, CERN Yellow Report No. 95-06, 1995, Vol. II, p. 879.

[22] D. Barber *et al.,* Nucl. Instrum. Methods Phys. Res., Sect. A **338**, 166 (1994).

[23] R. Assmann *et al.,* in *SPIN 2000: 14th International Spin Physics Symposium,* edited by Kichiji Hatanaka, Takashi Nakano, Kenichi Imai, and Hiroyasu Ejiri, AIP Conf. Proc. No. 570 (AIP, New York, 2001).

[24] Ya. S. Derbenev, A. M. Kondratenko, and A. N. Skrinsky, Part. Accel. **9**, 247 (1979).

[25] Desmond Barber (private communication).

[26] R. Assmann, in Ref. [3].

[27] R. Kleiss and H. Burkhardt, Comput. Phys. Commun. **81**, 372 (1994).

[28] K. Y. Ng, Fermilab Report No. Fermilab-Conf-00/142-T, 2000.

[29] E. Keil and W. Schnell, CERN Report No. TH-RF/69-48, 1969; D. Boussard, CERN Report No. Lab II/RF/Iny./75-2, 1975.

[30] A. Chao and J. Gareyte, SLAC Note No. SPEAR-197, 1976.

[31] CERN Report No. CERN-AC/96-01(LEP2), 1996.

[32] M. S. Zisman, S. Chattopadhay, and J. Bisognano, LBL Report No. LBL-21270, 1986.

[33] F. Sacherer, CERN Report No. CERN/MPS/BR 73-1, 1973; IEEE Trans. Nucl. Sci. **3**, 825 (1973).

[34] J. Butler (private communication).

[35] Parameters at other energies may be found on the web at http://www-ap.fnal.gov/~tsen/vllc_params.pdf

[36] The LEP Injector Study Group, CERN Report No. CERN-LEP/TH/83-29, 1983.

[37] G. Stange, IEEE Trans. Nucl Sci. **26**, 4146 (1979).

[38] ANL Report No. ANL-87-15 Annex, 1987.

[39] R. Noble (private communication).

[40] B. Brown (private communication.

[41] M. Derrick, H. Friedsam, A. Gorski, S. Hanuska, J. Jagger, D. Krakauer, J. Norem, E. Rotela, S. Sharma, L. Teng, K. Thompson, T. Sen, E. Chojnacki, and D. P. Barber, in *Proceedings of the Particle Accelerator Conference, New York, 1999* (Ref. [14]), p. 2635.

[42] Executive Summary of the M4 Working Group, in *2001 Snowmass Accelerator R&D Report,* available at http://www.hep.anl.gov/pvs/dpb/Snowmass.pdf

[43] O. Grobner (private communication).

[44] J. Norem and E. Keil, ANL Report No. ANL-HEP-CP-96-94, 1996.

[45] J. Norem, J. Jagger, S. Sharma, E. Keil, G. W. Foster, E. Malamud, E. Chojnacki, and D. Winn, in *Proceedings of the Particle Accelerator Conference, Vancouver, Canada, 1997* (IEEE, Piscataway, NJ, 1998), p. 363.

[46] C. W. Chen, *Magnetism and Metallurgy of Soft Magnetic Materials* (North-Holland, Amsterdam, 1977).

[47] *Metals Handbook, Desk Edition*, edited by J. R. Davis (The Materials Information Society, Materials Park, OH, 1998), 2nd ed.
[48] M. Sands, SLAC Report No. SLAC-121, 1970.
[49] H. Wiedemann, Nucl. Instrum. Methods **172**, 33 (1980).
[50] H. Wiedemann, *Particle Accelerator Physics II* (Springer-Verlag, Berlin, 1995).
[51] O. Grobner, A. G. Mathewson, H. Stori, P. Strubun, and R. Souchet, Vacuum **33**, 397 (1983).
[52] A. Chao, *Frontiers of Particle Beams*, Lecture Notes in Physics Vol. 296 (Springer-Verlag, Berlin, 1989), p. 51.
[53] H. Burkhardt, in *Proceedings of the Third Workshop on LEP Performance, Chamonix*, edited by J. Poole, CERN Report No. CERN SL/93-19, 1993.
[54] T. Sen and J. A. Ellison, Phys. Rev. Lett. **77**, 1051 (1996).